The Quantum-Geometric Correspondence: Three Axioms and Gravitational Decoherence at Order G

Marc Sperzel*

Independent Researcher

MSci Physics, King's College London

Abstract

Quantum mechanics and general relativity disagree about what spacetime is; we develop the hypothesis that they are complementary projections of a single underlying reality. Three primitive axioms carry the framework: Generalized Entropy (the area–entanglement ledger of Type II gravitational algebras), Entanglement Equilibrium (stationarity of that entropy for every small causal diamond, from which the Einstein equations follow as a theorem), and Modular Time (the diamond's modular flow is physical time, $K = 2\pi H_{\text{phys}} + \mathcal{O}(G^2)$—established in expectation values and solvable models, conjectured as a full operator identity). The falsifiable consequence is gravitational decoherence. The linearized Wheeler–DeWitt constraint entangles a matter superposition with its gravitational dressing; tracing the geometry decoheres the matter at $\Gamma_{\text{dec}} = C\,GM^2/(\hbar d)$ with $C \in [2/\pi, 1]$ and $C = 1$ for interferometric visibility, giving $\tau_{\text{dec}} = \hbar d/(GM^2) \approx 1.6$ ns for a 1 μg particle separated by 1 mm (point-mass convention). Standard perturbative quantum field theory, whose product initial state violates the constraint, predicts a G^2 rate $\sim 3 \times 10^{34}$ times slower—so even an order-of-magnitude measurement is decisive. In an exactly solvable constrained model a single object—the branch overlap—produces both behaviours, selected by the initial data alone: the product state must generate branch distinguishability dynamically (the G^2 channel), while the constrained state carries it statically, its conversion to a rate supplied by the relational structure that the third axiom makes precise. The mechanism extends to quantum fields via the stress-energy operator, and the same axioms underlie the holographic dark energy and emergent-gravity results of companion work. Experiment at the microgram scale decides the scaling.

Contents

*ORCID: 0009-0000-6252-3155. Email: me@marcsperzel.com

Part I

Framework

1 Introduction

Quantum mechanics describes nature as state vectors evolving unitarily in a fixed background spacetime; general relativity treats spacetime itself as dynamical. The clash is sharpest for a mass in spatial superposition: the semiclassical coupling $G_{\mu\nu} = (8\pi G/c^4)\langle T_{\mu\nu}\rangle$—the unique c-number bridge between the two theories—sources the metric of the *mean* stress tensor, a geometry realised in no branch of the superposition. Every laboratory mass placed in superposition therefore probes physics that neither theory alone describes, yet no complete theory of quantum gravity has converted this into a decisive laboratory test: string theory, loop quantum gravity, and asymptotic safety each capture part of the structure without a prediction at accessible scales.

Black-hole physics and holography point toward the resolution this paper develops. The Bekenstein–Hawking entropy [1, 2], the Ryu–Takayanagi prescription [3], and the ER=EPR conjecture [4] together indicate that entanglement does not merely correlate distant quantum systems but constitutes the fabric of spacetime itself. If so, quantum mechanics and general relativity are not competing descriptions requiring reconciliation but complementary projections of a single underlying reality. We call this the *Quantum-Geometric Correspondence*, and we develop it here to the point of a falsifiable number: a superposed mass entangles with its own gravitational field, and tracing the field decoheres the mass in $\tau_{\mathrm{dec}} = \hbar d/(GM^2)$—about 1.6 ns for a microgram over a millimetre.

The arc of this paper. This paper develops the Quantum-Geometric Correspondence from first principles and follows a single physical through-line from its axioms to a concrete, falsifiable laboratory prediction. The narrative has four movements.

(i) Axioms (Part I). We build the framework on three primitive axioms: Generalized Entropy, which fixes the entropy of a gravitating region to the area–entanglement ledger of its Type II observable algebra; Entanglement Equilibrium, the stationarity of that entropy for every small causal diamond, from which Einstein's equations follow as a theorem rather than being postulated; and Modular Time, the identification of the diamond's modular flow with physical time, which fixes the gravitational decoherence rate and is the framework's falsifiable commitment. From these we derive—as theorems, not further postulates—the Einstein equations, an Observer-Dependent Horizon Principle, a Holographic Information Bound, and the Semiclassical Duality Correspondence. The last of these is the physical heart of the framework: *a matter superposition does not source a single classical geometry, but becomes entangled with a superposition of gravitational field configurations.*

(ii) The key prediction: gravitational decoherence (Part II). When an experimenter measures only the matter and traces over the inaccessible geometry, this matter–geometry entanglement manifests as decoherence. The energy scale of the effect is the gravitational self-energy of the superposition, $E_{\mathrm{G}} = GM^2/d$ for a mass M split by a separation d, giving a decoherence time

$$\tau_{\mathrm{dec}} = \frac{\hbar d}{GM^2} = \frac{\hbar}{E_{\mathrm{G}}}. \tag{1}$$

For a 1 μg particle separated by 1 mm, this is $\tau_{\rm dec} \approx 1.6$ ns—fast enough to explain why macroscopic superpositions are never observed, yet within reach of next-generation matter-wave interferometry. This is the Diósi–Penrose energy scale, a hypothesis with strong physical motivation [5, 6].

(iii) Its G^1 rate (Part II). The decisive theoretical question is the power of G. Standard perturbative quantum field theory, applied to an unentangled product initial state, predicts a G^2 rate and decoherence times of order 10^{18} years for laboratory masses—effectively unobservable. We show that this product state *violates the linearized Wheeler–DeWitt constraint*: a mass must carry its own Newtonian field. Imposing the constraint forces an entangled initial state and replaces the noise-kernel mechanism (G^2) with a coherent-state-overlap mechanism (G^1). The central relation is $K = 2\pi H_{\rm phys} + \mathcal{O}(G^2)$, which we establish in expectation values and in solvable models and conjecture as a full operator identity (its operator-level status reduces to a single open construction; Sec. 9). The two predictions differ by $\sim 3 \times 10^{34}$ at the benchmark, so even an order-of-magnitude measurement is decisive.

(iv) Its coefficient and its reach (Part II and appendices). The G^1 scaling fixes the rate up to an $\mathcal{O}(1)$ coefficient C in $\Gamma_{\rm dec} = C\, E_{\rm G}/\hbar$. The Margolus–Levitin quantum speed limit bounds this coefficient to $C \in [2/\pi, 1]$, with the natural value $C = 1$ (Markovian dephasing, the Diósi master equation) and the floor $C = 2/\pi$ (the orthogonalization limit). Finally, the point-mass formula extends to quantum fields by replacing the mass density with the stress-energy operator, yielding decoherence rates for Fock-state superpositions and an application to inflationary perturbations.

The through-line is a single idea: the axioms entangle matter with geometry; the entanglement decoheres the matter; its energy scale is $E_{\rm G}$; its rate is G^1 once the Hamiltonian constraint is imposed; its coefficient is pinned to a narrow window; and it generalizes from particles to fields.

Status of the claims. We are careful throughout to distinguish what is established from what is motivated. The energy scale $E_{\rm G} = GM^2/d$ is established (it is classical gravitational self-energy). The G^1 scaling is *derived in linearized gravity within a controlled approximation* by imposing the Wheeler–DeWitt constraint; the extraction of a *rate* (linear-in-time decay) from this energy scale invokes the Hamiltonian constraint and the Page–Wootters mechanism for emergent time, and is the less rigorous step. The Diósi–Penrose identification of $E_{\rm G}/\hbar$ with the decoherence rate is a hypothesis with strong physical motivation, not a theorem. Standard perturbative QFT, which gives G^2, is correct for its (unconstrained) initial state; the two calculations answer different physical questions. The matter is ultimately empirical, and the framework makes a definite, falsifiable prediction.

Structure. Part I (Framework). Section 2 states the three primitive axioms and derives the horizon, holographic, and duality results. Section 3 treats the speculative Planck-scale extension: the minimum length, modified dispersion, and vacuum birefringence via the generalized-uncertainty route. **Part II (Gravitational decoherence).** Section 4 establishes the Diósi–Penrose mechanism and the energy scale $E_{\rm G}$. Section 5 reviews the unconstrained influence functional, locates its G^2 scaling in the product initial state, and states the experimental stakes. Section 6 imposes the Wheeler–DeWitt constraint on the Feynman–Vernon influence functional and derives the G^1 versus G^2 resolution. Section 7 extracts the rate, folds in the Margolus–Levitin coefficient bound, and gives the numerical prediction. **Part III.** Section 8 collects the testable predictions of the whole framework; Section 9 discusses connections, limitations, and outlook. The appendices provide the logical-independence proofs, the semiclassical mathematical framework, the entropic-action repackaging of Axiom II, self-consistency, the decoherence conventions and G-scaling arguments, the coherent-state overlap computation, the robustness of the $\mathcal{O}(G^2)$ corrections, the information-theoretic (Margolus–Levitin) bound, and the second-quantized field extension.

Series context. This is the canonical core paper of the Quantum-Geometric Correspondence series; it absorbs and unifies the previously separate treatments of the framework, the decoherence mechanism, the Wheeler–DeWitt rate, the information-theoretic bound, and the field-theoretic extension. Companion work applies the same axioms to holographic dark energy, $\rho_{\rm DE} = \alpha c^2 H^2/G$ with $\alpha \approx 0.082$ [7], and to emergent gravity and the MOND acceleration scale $a_0 = cH_0/(2\pi)$; we note these connections in passing (Section 9) but do not develop them here.

2 The Axiom Structure

The framework rests on *three primitive axioms*—Generalized Entropy, Entanglement Equilibrium, and Modular Time. They are the algebra, state, and time clauses of a single underlying statement: *the physical content of a region is the modular structure of its causal diamond, as seen by the region's observer.* The horizon, holographic, duality, and Einstein-equation results follow as theorems; the third axiom carries the framework's falsifiable content, and it alone is conjectural at the operator level. The three are logically independent (countermodels: Appendix A).

2.1 Axiom I: Generalized Entropy

Axiom I fixes what entropy is in the presence of gravity and how it behaves. Two established results motivate it. The resolution of the black hole information paradox [8]—via the Page curve [9], quantum extremal surfaces [10], and islands [11]—establishes that information is preserved beyond semiclassical gravity. Holography establishes *where* entropy resides: the Ryu–Takayanagi formula [3] equates the entanglement entropy of a boundary region with a bulk minimal-surface area over $4\ell_P^2$. The algebraic form of both statements is now a theorem family: when the gravitational constraints are imposed, the observables of a region dressed to an observer form a Type II von Neumann algebra—the crossed product of the field algebra by the observer's modular flow—whose entropy *is* the generalized entropy [12, 13].

Axiom 2.1 (Generalized Entropy)**.** *For a region bounded by a quantum extremal surface or causal horizon $\mathcal{X}$, with the gravitational constraints imposed, the physical observables form a Type II (crossed-product) algebra whose von Neumann entropy is the generalized entropy*

$$\boxed{S_{gen}(\mathcal{X}) = \frac{A(\mathcal{X})}{4\ell_P^2} + S_{ext}(\mathcal{X}) + const,} \tag{2}$$

defined up to an additive constant, where $A(\mathcal{X})$ is the proper area of the surface and S_{ext} is the von Neumann entropy of the exterior quantum fields. Moreover: (i) for the total state on a complete Cauchy slice, S_{gen} is invariant under evolution (global unitarity); (ii) for open subregions the Generalized Second Law holds, $\Delta S_{gen} \geq 0$ along future-directed horizon cuts;

(iii) the surface $\mathcal{X}$ is selected by the quantum-extremal-surface prescription $\partial_\lambda S_{gen} = 0$, taken as a postulate.

Three scope remarks keep the axiom honest. First, the split between the area term and S_{ext} is renormalization-scheme dependent; only the sum, its differences, and its monotonicity are physical, so the axiom asserts one well-defined ledger, not an exchange between two separately meaningful ones. Second, the area law $S = A/4\ell_P^2$ is the framework's irreducible geometric input: it is postulated here, not derived. Third, clause (i) is a statement about complete slices—it is ordinary unitarity, foliation-independent by construction; the framework makes no claim that the generalized entropy of a *subregion* is conserved (for an evaporating horizon it manifestly is not—that is the Page curve), and no downstream result requires such a claim.

The axiom's physical message is the entanglement–geometry correspondence: with the geometric term fixed to the area, a change in entanglement is necessarily accompanied by a change in geometry. A system in superposition entangling with its environment changes the corresponding geometric degrees of freedom—the gravitational decoherence of Part II.

2.2 Axiom II: Entanglement Equilibrium

Axiom II fixes which coupled matter–geometry configurations are self-consistent. Following Jacobson's thermodynamic route to the field equations [14], the statement is variational but refers directly to the generalized entropy of Axiom I, with no action functional inserted by hand.

Axiom 2.2 (Entanglement Equilibrium)**.** *Every small causal diamond D ($\ell_P \ll \ell \ll L_{curvature}$) is at entanglement equilibrium: the generalized entropy of Axiom I is stationary at fixed volume,*

$$\boxed{\delta S_{gen}(D) = 0.} \tag{3}$$

Theorem 2.3 (Einstein equations from Axioms I + II)**.** *For small causal diamonds, stationarity of the generalized entropy at fixed volume, together with the first law of entanglement $\delta S_{bulk} = \delta\langle K\rangle$ (Bisognano–Wichmann [15], with $K = 2\pi \int_{B_\ell} [(\ell^2 - r^2)/(2\ell)]\, T_{00}\, dV$ the diamond modular Hamiltonian) and the Raychaudhuri equation applied to the null boundary ($\delta A \propto -\ell^{d+1} G_{00}$), yields the semiclassical Einstein equations*

$$G_{\mu\nu} = \frac{8\pi G}{c^4}\,\langle T_{\mu\nu}\rangle. \tag{4}$$

The geometric and matter prefactors cancel exactly; no Einstein–Hilbert term is postulated.

The theorem is Jacobson's [14], and inherits his conditions (small diamonds, first-order variations, the cosmological constant entering as an integration constant). We emphasize what is and is not derived: the field equations follow from Axioms I and II *jointly*—the entropy–area relation itself is Axiom I's input, not a consequence. A second consequence of Axiom II is the local state: the equilibrium diamond satisfies the KMS condition at the modular temperature $\beta_{\text{mod}} = 2\pi$, which for accelerated observers is the Unruh temperature $\beta = 2\pi c/a$ and near horizons the Hawking temperature $\beta = 2\pi/\kappa$; in flat space far from horizons $\beta \to \infty$. The thermality is local and modular, not a global bath.

Remark 2.1 (The entropic action as equivalent repackaging). Earlier presentations of this framework stated Axiom II as an entropic action principle, extremizing $S[\rho, g] = \int d^4x\sqrt{-g}\,[\langle\hat{H}\rangle_\rho +$

$c^4R/(16\pi G) - s_{\text{vN}}(\rho)/\beta]$. That functional is retained in Appendix C as an *equivalent free-energy repackaging of the equilibrium statics*: its density-matrix variation reproduces the KMS/Gibbs condition and its metric variation reproduces the field equations once a covariant matter action is supplied. It is not a primitive postulate—the Einstein–Hilbert term it contains made the field equations an input rather than a result, and its variational content is the statics just described, not a dynamical law. Time evolution of quantum states is ordinary unitary quantum field theory on the self-consistent background; the framework's decoherence dynamics enters through Axiom III.

2.3 Axiom III: Modular Time

The first two axioms fix the entropy ledger and the self-consistent backgrounds; neither fixes the *rate* at which gravitational which-path information is registered. That rate is the content of the third axiom, which identifies the diamond's modular flow with its physical time. This is the framework's sharpest commitment and its falsifiable core.

Axiom 2.4 (Modular Time)**.** *For the diamond's observer, the modular flow of the constrained (Type II, observer-dressed) algebra at the KMS temperature $\beta_{mod} = 2\pi$ is physical time evolution. At the operator level,*

$$\boxed{K = 2\pi H_{phys} + \mathcal{O}(G^2).} \tag{5}$$

The consequence is gravitational decoherence at the G^1 rate: a mass superposition's branches are distinguished at the rate set by the modular gap,

$$\Gamma_{\text{dec}} = C\,\frac{E_{\text{grav}}}{\hbar}, \qquad E_{\text{grav}} = \frac{GM^2}{d}, \qquad C \in \left[\frac{2}{\pi}, 1\right], \tag{6}$$

with natural value $C = 1$ (the Diósi–Penrose rate [5, 6]). The window's lower edge is the Margolus–Levitin quantum speed limit read as a saturation statement—the earlier "Gravitational Information Axiom" presentation of this framework, which Axiom III supersedes: information transfer between matter and geometry at rate $dI_{S:G}/dt = 2E_{\text{grav}}/(\pi\hbar)$ is the $C = 2/\pi$ floor of Eq. (6).

We state the axiom's status plainly. The identity (5) is *proven* at the level of expectation values and in solvable models, and is *conjectured* as a full operator identity; Part II develops the supporting derivation (the linearized Wheeler–DeWitt constraint forces an entangled initial state, replacing the perturbative G^2 noise-kernel mechanism with the G^1 coherent-state-overlap mechanism), and Section 9 details what remains open. The commitment is unhedged: standard perturbative quantum field theory with an unconstrained product initial state predicts a G^2 rate; because that state violates the constraint, the framework predicts G^1 for every preparable superposition. Observation of G^2-timescale coherence—the joint M^2, d^{-1}, C-window test—falsifies Axiom III and with it the framework's distinctive content.

2.4 Derived: Observer-Dependent Horizons

Quantum and gravitational uncertainties are equivalent in scaling—a consequence of Axiom I with standard horizon thermodynamics, not a separate axiom. Applying the generalized entropy of Axiom I to a Rindler horizon, with the Heisenberg relation $\Delta E \cdot \Delta t \geq \hbar/2$ and the Unruh temperature $T = \hbar a/(2\pi c k_B)$ for an accelerating observer, gives the following.

Theorem 2.5 (Observer-Dependent Horizon Principle, scaling form)**.** *From Axiom I applied to Rindler horizons, together with horizon thermodynamics, quantum and gravitational uncertainties share the same dimensional content:*

$$\boxed{\Delta E \cdot \Delta t \geq \frac{\hbar}{2} \quad \Longleftrightarrow \quad a \cdot \Delta x \gtrsim c^2} \tag{7}$$

where a is proper acceleration; the precise $O(1)$ coefficient on the right-hand side is not fixed by the derivation and is conventionally written as $c^2/2$ to match the Heisenberg form (see Remark below).

Remark 2.2 (Scope of the $c^2/2$ coefficient)*.* The thermal-wavelength argument used in the derivation yields $a \cdot \Delta x \geq 2\pi c^2$, a factor of 4π larger than the conventional bound $c^2/2$. The $O(1)$ discrepancy is absorbed into "$\cdot O(1)$" without independent justification within the present framework, so Eq. (7) is best read as a statement of *equivalence in scaling*, not as a derivation of the specific Heisenberg coefficient from gravity.

An accelerating observer has a Rindler horizon at distance c^2/a; the gravitational uncertainty $a \cdot \Delta x \gtrsim c^2$ bounds the minimum distance from this horizon, and $\Delta E \cdot \Delta t \geq \hbar/2$ bounds the associated energy fluctuations. The derivation takes the Unruh result as established external physics: a framework that modifies it (doubly special relativity, for example) need not satisfy Eq. (7). Section 3 uses this principle to obtain the generalized uncertainty principle.

2.5 Derived: Holographic Information Bound

The holographic principle—the maximum entropy of a region is bounded by its boundary area, not its volume [16, 17, 18]—is here a theorem following from Axiom I and the generalized second law (GSL).

Theorem 2.6 (Holographic Bound)**.** *From Axiom I (Generalized Entropy) and the Generalized Second Law:*

$$\boxed{S_{\max} \leq \frac{A}{4\ell_P^2}} \tag{8}$$

Sketch. Axiom I fixes the geometric entropy to $A/(4\ell_P^2)$. The GSL requires S_{gen} to be non-decreasing along future horizon cuts. Combining these with the requirement that S_{matter} cannot exceed the horizon capacity yields the bound. □

The bound constrains the information content of spacetime regions and, applied to cosmological horizons, yields the holographic dark energy of companion work [7].

2.6 Derived: Semiclassical Duality Correspondence

The central physical result of the framework fixes how matter superpositions couple to geometry in the semiclassical regime. Axiom I ties entanglement to geometric area, so a change in quantum state is accompanied by a change in geometry; the Semiclassical Duality Correspondence makes this precise as a theorem following from Axioms I and II.

Proposition 2.7 (Semiclassical Matter-Geometry Entanglement)**.** *In the semiclassical regime, superpositions of matter states produce entangled matter-geometry states:*

$$\boxed{|\Psi\rangle = \sum_n c_n|\psi_n\rangle \quad \Longrightarrow \quad |\Psi_{total}\rangle = \sum_n c_n|\psi_n\rangle \otimes |\alpha^{(n)}\rangle} \tag{9}$$

where $|\alpha^{(n)}\rangle$ are gravitational coherent states with expectation value $\langle\alpha^{(n)}|\hat{h}_{\mu\nu}|\alpha^{(n)}\rangle = h^{(n)}_{\mu\nu}$ satisfying the linearized Einstein equations sourced by $|\psi_n\rangle$.

This is the essence of the Quantum-Geometric Correspondence: a matter superposition sources no single classical geometry, but correlates each branch with its geometric perturbation, leaving an entangled state in which matter and geometry cannot be described independently. The supporting mathematics—gravitational coherent states and the semiclassical validity regime—is developed in Appendix B. An external observer who traces over the geometric degrees of freedom, inaccessible to typical laboratory measurements, sees the matter state decohere: the gravitational decoherence of Part II, whose *rate* is fixed by Axiom III.

2.7 Speculative extension: Planck-scale phenomenology

Earlier presentations included a fourth statement—a Planck-scale interpolation $\mathcal{O}_{\text{unified}} = \rho_{\text{QM}}\, f(r/\ell_P) + \rho_{\text{GR}}\,[1-f]$—as a primitive axiom. It is not one here, for cause: wherever the Einstein equations (Theorem 2.3) hold, the two densities coincide and the interpolation is trivial; where they are asserted to fail, the interpolated source violates the contracted Bianchi identity, $\nabla^\mu T^{\text{eff}}_{\mu\nu} = (\langle T_{\mu\nu}\rangle - \frac{c^4}{8\pi G}G_{\mu\nu})\,\nabla^\mu f \neq 0$, exactly where the statement has content; and the radial profile singles out a frame. The minimum-length and modified-dispersion estimates of Section 3 therefore stand on the generalized-uncertainty-principle route through Theorem 2.5, carry explicit $O(1)$-coefficient and power-law uncertainty, and are presented as a speculative ultraviolet extension of the framework rather than consequences of its axioms.

2.8 Axiomatic Structure Summary

Primitive Axioms (independent, cannot be derived; the algebra, state, and time clauses of the diamond's modular structure):

Axiom	Content	Physical Basis
I	Generalized Entropy	Unitarity + holography (Type II algebras)
II	Entanglement Equilibrium	First law of entanglement
III	Modular Time	Thermal time; Wheeler–DeWitt constraint

Derived Results (theorems following from the axioms):

Result	Content	Derived From
Theorem 2.3	Einstein equations	Axioms I + II
Theorem 2.5	Observer-Dependent Horizons	Axiom I + horizon thermodynamics
Theorem 2.6	Holographic Bound $S \leq A/(4\ell_P^2)$	Axiom I + GSL
Prop. 2.7	Semiclassical Duality Correspondence	Axioms I + II
$\Gamma_{\text{dec}} = C\, E_{\text{grav}}/\hbar$	Gravitational decoherence rate	Axiom III

Axiom III is the framework's conjectural clause: Eq. (5) is proven in expectation values and solvable models and conjectured as an operator identity, so the rate row inherits that status; it is also the clause experiment tests. The three primitive axioms are logically independent: each can be violated while the others hold, as we demonstrate through explicit countermodels in Appendix A.

Remark 2.3 (Relation to earlier formulations). Two earlier presentations map onto the present one. (i) A six-statement enumeration split Axiom I into separate "Information Conservation" and "Entanglement–Geometry Correspondence" statements and listed the horizon and holographic results alongside the axioms; that structure is recovered here with the split statements as facets of Axiom I and the remainder as Theorems 2.5 and 2.6. (ii) The v2.0 minimal formulation stated Axiom II as the entropic action (here Remark 2.1: an equivalent repackaging of the equilibrium statics), included the Planck-scale interpolation as its third axiom (here Section 2.7: a speculative extension, for the reasons stated there), stated a closed-system conservation clause for the generalized entropy of subregions (withdrawn here; clause (i) of Axiom I is the global-slice statement that was actually in use), and carried the decoherence rate as a separate "Gravitational Information Axiom" hypothesis (here promoted to Axiom III, making the framework's falsifiable commitment part of its axiomatic identity). No numerical prediction changes under the reformulation.

3 Speculative Ultraviolet Extension: Planck-Scale Phenomenology

The material of this section is the framework's speculative ultraviolet extension (Section 2.7): it is not a consequence of the three primitive axioms. Three Planck-scale signatures survive on the generalized-uncertainty-principle route through the observer-dependent horizon principle (Theorem 2.5)—a minimum measurable length, modified dispersion relations, and vacuum birefringence—each carrying an explicit $O(1)$-coefficient and power-law uncertainty. Where an interpolation function between quantum and geometric descriptions was invoked in earlier presentations, it is a heuristic device, not an axiom.

3.1 The generalized uncertainty principle and the minimum length

Heisenberg's relation $\Delta x \cdot \Delta p \geq \hbar/2$ places no lower bound on position uncertainty alone: arbitrarily precise localization is allowed at the cost of momentum uncertainty. Gravity removes this freedom—localizing a particle concentrates energy until the density forms a black hole and the measurement loses meaning. The observer-dependent horizon principle expresses the same obstruction algebraically: the modified commutator

$$\boxed{[\hat{x}, \hat{p}] = i\hbar \left(1 + \beta_{\mathrm{GUP}} \frac{\ell_P^2 \hat{p}^2}{\hbar^2}\right)} \tag{10}$$

with β_{GUP} a dimensionless parameter of order unity. The Robertson relation $\Delta A \cdot \Delta B \geq |\langle [\hat{A}, \hat{B}] \rangle|/2$, applied to (10) with $\langle \hat{p}^2 \rangle \approx (\Delta p)^2$ for a minimum-uncertainty state, gives the generalized uncertainty principle (GUP)

$$\boxed{\Delta x \geq \frac{\hbar}{2\Delta p} + \frac{\beta_{\mathrm{GUP}} G \Delta p}{2c^3}}\,, \tag{11}$$

the quantum contribution dominant at low momenta, the gravitational at high momenta. Minimizing over Δp gives $\Delta p_{\mathrm{opt}} = \hbar/(\sqrt{\beta_{\mathrm{GUP}}}\,\ell_P)$ and

$$\boxed{\Delta x_{\min} = \sqrt{\beta_{\mathrm{GUP}}}\,\ell_P \approx (1.4 \pm 0.5)\,\ell_P \approx (2.3 \pm 0.8) \times 10^{-35}\ \mathrm{m}} \tag{12}$$

using $\beta_{\mathrm{GUP}} = 2$ with estimated range 1–4: no procedure localizes an object below Planck precision. This is a property of nature, not an experimental limitation. It is sometimes read as evidence for discrete spacetime, but the present framework is agnostic—the minimum length emerges from the uncertainty principle, not from explicit discreteness.

3.2 Modified dispersion and photon time delay

The modified commutator modifies the dispersion relation. To leading order,

$$\boxed{E^2 = p^2 c^2 \left(1 + \xi \frac{p^2 \ell_P^2}{\hbar^2}\right) + m^2 c^4} \tag{13}$$

where $\xi = \beta_{\mathrm{GUP}} \sim O(1)$; the $(p\ell_P/\hbar)^2$ suppression makes the correction negligible for ordinary particles but potentially relevant for ultra-high-energy photons. For massless particles, $v = dE/dp$ yields

$$v = c\left(1 - |\xi| \frac{E^2}{E_P^2}\right), \tag{14}$$

with $E_P = \sqrt{\hbar c^5/G} \approx 1.22 \times 10^{19}$ GeV and the subluminal convention ($\xi > 0$) adopted to match observational constraints: higher-energy photons travel slower, by one part in 10^{38} at GeV energies. Two photons of energies E_1, E_2 emitted simultaneously at distance L arrive separated by

$$\Delta t = \xi \frac{E_1^2 - E_2^2}{E_P^2} \cdot \frac{L}{c}\,. \tag{15}$$

For a gamma-ray burst at cosmological distance ($L \sim 10^{26}$ m) with GeV photons, $\Delta t \sim 2 \times 10^{-21}$ s—far below any timing resolution; a linear-dispersion scenario at the same Planck scale gives $\Delta t \sim 0.03$ s for the same burst, within reach of current instruments. The quadratic suppression is thus both the framework's signature and the price of that signature. The E^2 scaling discriminates among alternatives: some loop-quantum-gravity scenarios predict E^1, other effective theories E^3 or higher. Gamma-ray-burst timing excludes Planck-scale *linear* dispersion [19]; the same data constrain the quadratic coefficient only many orders of magnitude above unity, so the $\mathcal{O}(1)$ prediction for ξ is consistent with—but far from tested by—current observations.

3.3 Vacuum birefringence from non-commutative spacetime

A further extension promotes the modified position–momentum commutator to non-commutativity of the coordinates themselves,

$$[\hat{x}^\mu, \hat{x}^\nu] = i\theta^{\mu\nu}, \qquad \theta^{\mu\nu} \sim \ell_P^2\, \Theta^{\mu\nu}, \tag{16}$$

with $\Theta^{\mu\nu}$ a dimensionless antisymmetric tensor and the magnitude set by the Planck area on dimensional grounds. The tensor defines preferred spacetime directions, breaking Lorentz invariance: left- and right-handed circularly polarized photons couple differently to the non-commutative structure and propagate at different speeds—vacuum birefringence. The polarization plane rotates by an energy- and distance-dependent angle whose scaling is fixed to E^3 by symmetry (the leading E^1 and E^2 corrections are forbidden in this framework):

$$\Delta\phi \approx \Delta\eta \left(\frac{E}{E_P}\right)^3 \cdot \frac{L}{\ell_P}\,, \tag{17}$$

with $|\Delta\eta| \sim O(1)$. For a burst at redshift $z \sim 2$–3 ($L \sim 10^{26}$ m $\approx 10^{61}\,\ell_P$) and $E \sim 10$ MeV photons,

$$\Delta\phi \sim 5 \times 10^{-3} \text{ rad} \sim 0.3^\circ, \tag{18}$$

at the edge of next-generation gamma-ray polarimetry. The E^3 scaling again discriminates: Myers–Pospelov effective theory predicts E^2 birefringence, and the Standard Model Extension includes E^1 and E^2 operators. Current observations detect no significant birefringence, with limits not yet stringent enough to constrain E^3 effects at the predicted level [20]; IXPE [21] and future dedicated polarimeters will tighten them. A positive detection would signal Planck-scale structure; continued non-detection bounds $\Delta\eta$ and falsifies parameter ranges.

Part II
Gravitational Decoherence

4 The Diósi-Penrose Mechanism

Tracing over the geometry that a matter superposition becomes entangled with (the Semiclassical Duality Correspondence, Proposition 2.7) decoheres the matter; the Diósi-Penrose hypothesis fixes the rate to the classical gravitational self-energy of the superposition divided by $\hbar$. The microscopic justification of the resulting G^1 rate follows in Sections 6 and 7.

4.1 Gravitational self-energy

The Diósi-Penrose gravitational self-energy measures the difference between the two geometric configurations:

$$E_G = \frac{G}{2} \int\int \frac{[\rho_1(\mathbf{x}) - \rho_2(\mathbf{x})][\rho_1(\mathbf{y}) - \rho_2(\mathbf{y})]}{|\mathbf{x} - \mathbf{y}|} d^3x\, d^3y \tag{19}$$

where ρ_1 and ρ_2 are the mass densities in the two branches of the superposition. For two genuine point masses of mass M separated by d, the double integral reduces to the cross-term

$$E_G = \frac{GM^2}{d}. \tag{20}$$

Equation (20) is the canonical benchmark scale throughout this paper. Two clarifications matter for finite-size particles. First, GM^2/d is the *cross-term* of Eq. (19) — the branch self-energies (formally infinite for true point masses) cancel in the difference; it is *not* the $d \gg R$ limit of an extended particle. Second, for a uniform sphere of radius R split by $d \geq 2R$, the full self-energy Eq. (19) *saturates* at $E_G \to \frac{6}{5}GM^2/R = 1.2\,GM^2/R$, set by the particle size R rather than the separation d (the cross-term GM^2/d is recovered by *dropping* the branch self-terms, not by taking $d \gg R$). At the reference benchmark used below ($M = 1$ μg, $d = 1$ mm; for silica $R \approx 48$ μm, so $d/2R \approx 10$) the two forms differ by a factor $\sim$24. The benchmark $\tau_{\text{dec}} = \hbar d/(GM^2) \approx 1.6$ ns is therefore quoted in the point-mass convention; the finite-size saturated rate, and its consequences for the orientation-dependent BMV/QGEM visibility, are developed in the companion BMV paper of this series. The choice of convention does not affect the G^1-versus-G^2 *scaling* question, which is this paper's subject.

4.2 The Diósi-Penrose hypothesis

For a mass distribution in a superposition of two configurations with branch densities $\rho_1(\mathbf{x}), \rho_2(\mathbf{x})$, the self-energy (19) is the gravitational interaction energy between the excess mass in one branch and the deficit in the other; for two point masses it reduces to $E_G = GM^2/d$.

Hypothesis 4.1 (Diósi-Penrose)**.** *The gravitational self-energy sets the decoherence rate,*

$$\Gamma_{dec} = \frac{E_G}{\hbar}, \tag{21}$$

the gravitational energy scale converted to a frequency by Planck's constant.

The prescription (21) introduces no coupling constant beyond G, no perturbative expansion, and no detail of the mediating degrees of freedom: it treats the gravitational self-energy as fundamental and converts it to a rate by the energy–frequency relation.

For a mass M in spatial superposition over distance d the initial state is

$$|\Psi(t=0)\rangle = \frac{1}{\sqrt{2}}\left(|\mathbf{r}_1\rangle + |\mathbf{r}_2\rangle\right), \quad |\mathbf{r}_1 - \mathbf{r}_2| = d. \tag{22}$$

We work in the regime where the Newtonian approximation is valid ($GM/(c^2 d) \ll 1$), the superposition separation exceeds the particle size ($d \gg r$), and environmental decoherence from photons, gas molecules, and thermal radiation has been suppressed through high vacuum and cryogenic temperatures.

Under these conditions the off-diagonal elements of the density matrix decay exponentially,

$$\rho_{12}(t) = \rho_{12}(0)e^{-\Gamma t} = \rho_{12}(0)e^{-t/\tau_{\text{dec}}}, \tag{23}$$

where the decoherence time is the inverse of the rate given by Eq. (21). For a point mass, this yields

$$\boxed{\tau_{\rm dec} = \frac{\hbar d}{C\,GM^2}}, \qquad \Gamma_{\rm dec} = C\,\frac{GM^2}{\hbar d}, \tag{24}$$

with C of order unity. The value of C depends on details the Diósi-Penrose hypothesis alone does not specify: the geometry of the mass distribution, the regularization of the point-particle self-energy, and the exact map from energy scale to rate. Section 7 bounds C by the Margolus-Levitin quantum speed limit to the window $[2/\pi, 1]$, with natural value $C = 1$ (Markovian dephasing). All explicit rate formulas in this paper set $C = 1$; the residual uncertainty in C bears on absolute timescales, not on the scaling relations $\tau \propto M^{-2}$, $\tau \propto d$, $\Gamma \propto G^1$, which are the primary experimental targets.

4.3 Features of the timescale

The formula (24) distinguishes gravitational decoherence from other mechanisms in three respects.

It requires both $\hbar$ and G. Neither classical gravity alone nor quantum mechanics without gravity produces this timescale; $\hbar d/(GM^2)$ is the unique timescale of correct dimension constructible from the available quantities.

It is temperature-independent. The self-energy depends only on the mass distribution, not on the thermal state of system or environment, so gravitational decoherence persists at absolute zero where thermal decoherence vanishes. A decoherence rate approaching a constant floor as temperature is reduced, rather than continuing to decrease, signals gravity as the cause.

It is vacuum-independent. Decoherence from scattered photons or gas molecules is suppressed by improving the vacuum; gravitational decoherence is not, operating with no photons, gas, or thermal radiation—only the gravitational field. Decoherence persisting at the gravitational rate as vacuum quality improves supports the hypothesis.

4.4 Numerical estimate and mass scaling

For $M = 1\ \mu\text{g} = 10^{-9}$ kg in superposition over $d = 1\ \text{mm} = 10^{-3}$ m, Eq. (24) with $C = 1$ gives

$$\begin{aligned}
\tau_{\rm dec} &= \frac{\hbar d}{GM^2} \\
&= \frac{(1.05\times10^{-34}\ \text{J}\cdot\text{s})(10^{-3}\ \text{m})}{(6.67\times10^{-11}\ \text{m}^3\text{kg}^{-1}\text{s}^{-2})(10^{-9}\ \text{kg})^2} \\
&\approx 1.6\times10^{-9}\ \text{s}.
\end{aligned} \tag{25}$$

A microgram particle delocalized over a millimeter decoheres in about a nanosecond—fast enough to explain why such superpositions are never observed, slow enough to remain within reach of future experiments.

The M^{-2} scaling is steep: doubling the mass quarters the coherence time, so macroscopic objects decohere almost instantaneously. A 1 mg particle gives $\tau_{\rm dec} = 1.6\times10^{-15}$ s, a 1 g particle 1.6×10^{-21} s, and human scales (70 kg at 1 m) of order 10^{-28} s, far shorter than any process could create such a superposition.

4.5 Falsification criteria

The Diósi-Penrose hypothesis is falsified by any of the following:

1. If coherence persists for times exceeding the predicted τ_{dec} by more than a factor of 10^3, accounting for the uncertainty in the coefficient C, the hypothesis in its current form would be ruled out.

2. If decoherence rates are observed to scale as G^2 rather than G^1—that is, if rates are approximately 3×10^{34} times slower than predicted (for the $1\,\mu$g, $1\,$mm benchmark)—the hypothesis would be falsified in favor of standard quantum field theory predictions.

3. If decoherence rates depend strongly on temperature or vacuum quality, scaling down as these are improved rather than approaching a constant floor, then the observed decoherence is environmental rather than gravitational.

4. If decoherence rates scale as M^{-1} rather than M^{-2}, this would favor Károlyházy's model over Diósi-Penrose, providing discrimination between different proposed gravitational decoherence mechanisms.

5 The Standard Feynman-Vernon Influence Functional

The standard, unconstrained derivation of gravitational decoherence via the Feynman-Vernon influence functional [22, 23] yields G^2 scaling; the source of that scaling is the product-state initial condition, which the constrained calculation of Section 6 removes to obtain G^1. A recent closed-time-path computation of graviton-mediated decoherence by a dilute gas [24], built on the same factorized initial state, confirms the G^2 character of the unconstrained channel.

5.1 Setup

A point mass M with center-of-mass coordinate q couples to the quantized linearized gravitational field $h_{\mu\nu}$. The total action separates into three pieces,

$$S[q,h] = S_M[q] + S_G[h] + S_{\text{int}}[q,h], \tag{26}$$

where S_M is the free matter action, S_G is the free graviton action (the linearized Einstein-Hilbert action for $h_{\mu\nu}$), and the interaction takes the form

$$S_{\text{int}}[q,h] = \frac{\kappa}{2} \int d^4x\, T^{\mu\nu}(x;q)\, h_{\mu\nu}(x), \tag{27}$$

with coupling constant

$$\kappa = \sqrt{\frac{32\pi G}{c^4}}\,. \tag{28}$$

The stress-energy tensor $T^{\mu\nu}$ depends on the matter trajectory $q(t)$, and $\kappa \propto \sqrt{G}$ is the perturbative expansion parameter.

5.2 The reduced density matrix

The reduced density matrix of the mass, after tracing over the gravitational field, takes the Feynman-Vernon path-integral form [22],

$$\rho_M(q_f, q'_f; t) = \int \mathcal{D}q^+ \, \mathcal{D}q^- \; \exp\Big(\frac{i}{\hbar}[S_M[q^+] - S_M[q^-]]\Big)\, \mathcal{F}[q^+, q^-]\, \rho_M(q_i, q'_i; 0), \tag{29}$$

where q^+ and q^- are the forward and backward paths of the mass, and the influence functional $\mathcal{F}$ encodes the entire effect of the gravitational environment:

$$\mathcal{F}[q^+, q^-] = \int \mathcal{D}h^+ \, \mathcal{D}h^- \; \exp\Big(\frac{i}{\hbar}[S_G[h^+] + S_{\text{int}}[q^+, h^+] - S_G[h^-] - S_{\text{int}}[q^-, h^-]]\Big)\, \rho_E(h_i, h'_i). \tag{30}$$

Here ρ_E is the initial state of the gravitational field.

5.3 The product-state assumption

The standard treatment [22, 23, 25, 26] takes the initial state to be a product,

$$|\Psi(0)\rangle = |\psi_{\text{matter}}\rangle \otimes |0_{\text{grav}}\rangle\,, \tag{31}$$

with $|0_{\text{grav}}\rangle$ the graviton vacuum—the usual open-systems assumption that system and environment begin unentangled and the environment in its ground state.

The graviton path integral is then Gaussian and the influence functional is exact. With the difference variable $\Delta q(t) = q^+(t) - q^-(t)$, the imaginary part of the influence phase—which produces decoherence—is the noise-kernel form [23, 25]

$$\text{Im}\,\Phi[q^+, q^-] = \frac{1}{2\hbar}\int_0^t ds \int_0^t ds' \; \Delta T^{\mu\nu}(s)\; N_{\mu\nu\alpha\beta}(s - s')\; \Delta T^{\alpha\beta}(s'), \tag{32}$$

where $\Delta T^{\mu\nu}(s) = T^{\mu\nu}(q^+(s)) - T^{\mu\nu}(q^-(s))$ is the stress-energy difference between the two paths, and $N_{\mu\nu\alpha\beta}$ is the graviton noise kernel—the symmetrized (Hadamard) two-point function of the gravitational field:

$$N_{\mu\nu\alpha\beta}(x, x') = \frac{\kappa^2}{4}\,\big\langle\{h_{\mu\nu}(x),\, h_{\alpha\beta}(x')\}\big\rangle_0\,. \tag{33}$$

5.4 G-counting: why the standard result scales as G^2

The G-scaling is most transparent in the equivalent master-equation formulation [25],

$$\frac{d\hat{\rho}_M}{dt} = -\frac{1}{\hbar^2}\int_0^t dt' \; \text{Tr}_{\text{grav}}\big[H_{\text{int}}(t),\, [H_{\text{int}}(t'),\, \hat{\rho}_M \otimes |0\rangle\langle 0|]\big], \tag{34}$$

with $H_{\text{int}} = (\kappa/2)\int d^3x\, T^{\mu\nu} h_{\mu\nu}$. The double commutator carries two insertions of H_{int}, each with one factor $\kappa \propto \sqrt{G}$, hence $\kappa^2 \propto G$. The graviton-vacuum trace produces the Hadamard function $\langle 0|\{h_{\mu\nu}(x), h_{\alpha\beta}(x')\}|0\rangle$, which for the canonically normalized field carries no explicit G. Coupling and trace alone therefore give G^1.

The second power enters through the contraction of the noise kernel with $\Delta T^{\mu\nu} \propto M$ and the integration over the graviton spectral density: for a non-relativistic mass the frequency integrals supply the additional G via the Newtonian potential $\Phi_N \propto GM/r$ connecting the two vertices (one emission, one absorption). The net rate of Anastopoulos and Hu [25] and Blencowe [26] is therefore $\Gamma_{\mathrm{QFT}} \propto G^2$, of the form

$$\boxed{\Gamma_{\mathrm{QFT}} \sim \frac{G^2 M^4}{\hbar^3 d^2}} \tag{35}$$

(suppressing order-unity prefactors and factors of c). For a 1 μg mass separated by 1 mm, $\tau_{\mathrm{QFT}} = 1/\Gamma_{\mathrm{QFT}} \sim 10^{18}$ years—effectively infinite, far beyond any foreseeable reach.

5.5 Identification of the critical assumption

The G^2 scaling traces directly to the product-state assumption (31). In the noise-kernel mechanism the two branches emit slightly different graviton fields, and the growing distinguishability of those fields degrades coherence. The process is *dynamical*: matter-field entanglement must be *generated* from zero through the interaction. Entanglement generation runs at $H^2_{\mathrm{int}} \propto G$, and propagation of the emitted gravitons through the vacuum adds a second G, giving G^2.

The product state (31) violates the linearized Wheeler-DeWitt constraint: a mass at position q must carry its Newtonian field, so the graviton vacuum $|0_{\mathrm{grav}}\rangle$ is not a physical state for a system containing matter. The constraint forces an *entangled* initial state, each branch dressed by its own coherent field configuration. Section 6 imposes the constraint and replaces the noise-kernel mechanism (dynamical entanglement generation, G^2) with a coherent-state-overlap mechanism (pre-existing entanglement manifestation, G^1): the rate is set by how fast the pre-existing dressing of the two branches becomes distinguishable, not by how fast gravitons are emitted.

5.6 Experimental discrimination and its stakes

The two rates follow from different initial states, not different approximation schemes: G^2 from the unconstrained product state, G^1 from the Wheeler-DeWitt-constrained entangled state. The framework commits to the G^1 rate: imposing the Hamiltonian constraint on the physical initial state is not optional within the theory, so G^1—not G^2—is its prediction. The two differ by $(M_P/M)^2(d/\ell_P) \approx 3 \times 10^{34}$ at the $1\,\mu$g, $1\,$mm benchmark ($\sim 10^{-9}$ s versus $\sim 10^{18}$ years), so experiment discriminates them even with substantial uncertainty. Decoherence in the nanogram-to-microgram range on millisecond-to-nanosecond timescales confirms the prediction; coherence persisting to the G^2 timescale falsifies it, leaving the standard product-state QFT result in its place. The G^2 rate is the alternative the experiment is set against, not a second prediction this framework endorses.

The outcomes carry opposite implications. G^1 scaling would mean the classical gravitational self-energy enters quantum dynamics in a way perturbative graviton exchange does not capture. G^2 scaling would make gravity "just another quantum field" at the level of decoherence: the same Lindblad mechanism as any environmental coupling, experimentally irrelevant timescales, and the classicality of macroscopic objects left entirely to conventional environmental decoherence. Whether gravity requires special treatment in quantum mechanics, or quantizes like other fields, is among the central open problems in theoretical physics; a measured gravitational decoherence rate bears directly on it.

6 The Constrained Influence Functional

Imposing the Wheeler-DeWitt constraint on the Schwinger-Keldysh path integral changes *both* the initial state and the structure of the functional integral, replacing the noise-kernel mechanism of Section 5 (G^2) with a coherent-state overlap mechanism (G^1).

6.1 The Wheeler-DeWitt constraint in linearized gravity

Physical states of canonical quantum gravity satisfy the Hamiltonian constraint [27]:

$$\hat{H}_{\text{total}} \, |\Psi_{\text{phys}}\rangle = 0 \, . \tag{36}$$

In the linearized (Newtonian) limit, the total Hamiltonian decomposes as $\hat{H}_{\text{total}} = \hat{H}_{\text{matter}} + \hat{H}_{\text{grav}} + \hat{H}_{\text{int}}$, and the constraint reduces to the operator Poisson equation:

$$\nabla^2 \hat{\Phi}(\mathbf{x}) = 4\pi G \, \hat{\rho}(\mathbf{x}) \, , \tag{37}$$

which determines the Newtonian potential $\hat{\Phi}$ from the mass density $\hat{\rho}$. Equation (37) is not a field equation but a *constraint* that restricts the physical Hilbert space: any state violating it is unphysical and projected out.

Remark 6.1. The constraint (37) is the gravitational analog of Gauss's law $\nabla \cdot \hat{\mathbf{E}} = \hat{\rho}_e/\epsilon_0$ in QED, with one structural difference: Gauss's law constrains a *spatial* degree of freedom (the longitudinal electric field), while the Hamiltonian constraint (36) constrains the *temporal* evolution. This distinction—temporal versus spatial constraint—makes gravity special for decoherence (Section 6.7).

6.2 The constrained initial state

The constraint (37) fixes the allowed quantum states of a mass in spatial superposition: each branch carries its own coherent gravitational field, and the product state of the standard calculation is excluded.

6.2.1 Single branch

For a point mass M localized at position $\mathbf{x}_A$, the constraint uniquely determines the gravitational potential:

$$\Phi_{\text{cl}}[\mathbf{x}_A](\mathbf{x}) = -\frac{GM}{|\mathbf{x} - \mathbf{x}_A|} \, . \tag{38}$$

In the quantum theory, the gravitational field must be in the state that reproduces this classical potential in expectation value while minimizing the field energy—a *coherent state*:

$$|\mathbf{x}_A\rangle_{\text{matter}} \;\longrightarrow\; |\mathbf{x}_A\rangle \, |\Phi_A\rangle = |\mathbf{x}_A\rangle \; \hat{D}(\alpha_A) \, |0\rangle \; , \tag{39}$$

where $\hat{D}(\alpha) = \exp\!\left(\int d^3k \, [\alpha(\mathbf{k}) \, \hat{a}^\dagger_{\mathbf{k}} - \alpha^*(\mathbf{k}) \, \hat{a}_{\mathbf{k}}]\right)$ is the Glauber displacement operator and the coherent-state amplitude is

$$\alpha_A(\mathbf{k}) = -\frac{4\pi GM}{k^2} \cdot \frac{e^{-i\mathbf{k}\cdot\mathbf{x}_A}}{\sqrt{2\hbar\omega_k}} \, , \tag{40}$$

with $\omega_k = c|\mathbf{k}|$ for relativistic gravitons. This is the standard result for a quantum field coupled linearly to a classical source [28], applied to linearized gravity. The coherent state is the unique minimum-uncertainty state satisfying the constraint at $O(G)$; graviton-squeezing corrections arise only at $O(G^2)$ with squeezing parameter $r \sim GM/(c^2 d) \sim 7 \times 10^{-34}$ (Appendix H).

6.2.2 Superposition

For a mass prepared in a spatial superposition $(|L\rangle + |R\rangle)/\sqrt{2}$, linearity of the constraint demands that each branch carry its own gravitational field. The physical state is therefore

$$\boxed{|\Psi_{\text{phys}}\rangle = \frac{1}{\sqrt{2}}(|L\rangle\,|\Phi_L\rangle + |R\rangle\,|\Phi_R\rangle)\,,} \tag{41}$$

where $|\Phi_A\rangle = \hat{D}(\alpha_A)\,|0\rangle$ with $\alpha_A(\mathbf{k})$ given by (40). This state is *necessarily entangled* between matter and geometry.

6.2.3 The product state is unphysical

The initial state of the standard Feynman-Vernon calculation, $|\psi_{\text{matter}}\rangle \otimes |0_{\text{grav}}\rangle$, *violates* the constraint (37): the gravitational field sits in the vacuum regardless of the matter configuration, so $\hat{\Phi}$ and $\hat{\rho}$ are uncorrelated, while the constraint demands perfect correlation. The product state therefore answers the perturbative question "at what rate does a bare, undressed mass become entangled with the graviton field?"—not the physical question "given that the constraint has already entangled the mass with its gravitational field, at what rate does this pre-existing entanglement cause operational decoherence?"

The product state $|\psi_{\text{matter}}\rangle \otimes |0_{\text{grav}}\rangle$ used in the standard Feynman-Vernon calculation **violates the Wheeler-DeWitt constraint**. The constraint demands the entangled state (41), in which each branch of the superposition carries its own coherent gravitational field. This single modification—replacing the product initial state with the constraint-entangled state—changes the G-scaling of the decoherence rate from G^2 to G^1.

6.3 Incorporating the constraint into the path integral

In the ADM formalism, the Hamiltonian constraint is enforced on the Schwinger-Keldysh path integral by integrating over the lapse function N, which acts as a Lagrange multiplier [27, 29]:

$$\int \mathcal{D}N\ \exp\!\Big(-\frac{i}{\hbar}\int dt\ N\,\hat{\mathcal{H}}_\perp\Big) = \delta[\hat{\mathcal{H}}_\perp]\,. \tag{42}$$

The constrained Schwinger-Keldysh functional integral for the reduced matter density matrix is obtained by inserting delta-function projectors onto the constraint surface [29, 30]:

$$\begin{aligned}
\rho_M(q_f, q_f'; t) = \int dq_i\, dq_i' \int \mathcal{D}q^+ \mathcal{D}q^- \int dh_f \int \mathcal{D}h^+ \mathcal{D}h^- \\
&\times\ \delta[\mathcal{C}(h^+, q^+)]\ \delta[\mathcal{C}(h^-, q^-)] \\
&\times\ \exp\Big(\frac{i}{\hbar}\left[S[q^+, h^+] - S[q^-, h^-]\right]\Big) \\
&\times\ \delta(h_f^+ - h_f)\, \delta(h_f^- - h_f)\ \rho_0(q_i, q_i'; h_i, h_i')\,,
\end{aligned} \tag{43}$$

where:

- $q^\pm$ and $h^\pm$ are the forward/backward matter and gravitational field paths, respectively;
- $\mathcal{C}(h, q) \equiv \nabla^2\Phi - 4\pi G\, \rho_q$ is the constraint functional;
- $\delta[\mathcal{C}(h^+, q^+)]$ and $\delta[\mathcal{C}(h^-, q^-)]$ enforce the constraint independently on each branch of the closed-time-path contour;[1]
- ρ_0 is the initial state—now the constrained, entangled state (41), *not* a product state.

6.4 Solving the constraint: ADM decomposition

The linearized gravitational field decomposes into three sectors that play distinct roles under the constraint [27]:

$$h_{\mu\nu} = \underbrace{\Phi}_{\text{Newtonian (scalar)}} + \underbrace{h_{ij}^{\mathrm{TT}}}_{\text{transverse-traceless}} + (\text{gauge modes})\,, \tag{44}$$

1. **Newtonian sector** (Φ): The constraint $\nabla^2\Phi = 4\pi G\rho_q$ *completely determines* Φ from the matter configuration at each time slice. For boundary conditions $\Phi \to 0$ at infinity, the solution is unique: $\Phi^\pm(\mathbf{x}, t) = \Phi_{\mathrm{cl}}[q^\pm(t)](\mathbf{x})$. The functional integral over Φ collapses: this sector has *no independent quantum fluctuations*. The constraint eliminates precisely those gravitational degrees of freedom that would normally contribute to the noise kernel.

2. **Transverse-traceless sector** (h_{ij}^{TT}): These two propagating polarizations (gravitational waves) satisfy $\Box\, h_{ij}^{\mathrm{TT}} = (16\pi G/c^4)\, T_{ij}^{\mathrm{TT}}$. For *static* masses in superposition, the transverse-traceless source vanishes: $T_{ij}^{\mathrm{TT}} = 0$ (gravitational wave emission requires time-varying quadrupole moments). Therefore the TT modes remain in the vacuum state and contribute no decoherence.

3. **Gauge modes**: Pure gauge in linearized gravity; eliminated by gauge fixing.

After solving the constraint, the gravitational field path integral *disappears* for the Newtonian sector: the potential on each branch is a deterministic functional of the matter path, and the

[1] The Faddeev-Popov determinant $\det(\nabla^2)$ associated with the constraint is field-independent for the Poisson equation with fixed boundary conditions, and cancels between the forward and backward paths of the Schwinger-Keldysh contour.

TT sector decouples from static sources. The effective action for the matter is

$$S_{\text{eff}}[q] = S_M[q] + S_{\text{grav-self}}[q]\,, \qquad S_{\text{grav-self}}[q] = -\frac{G}{2}\int dt \int d^3x\, d^3y\, \frac{\rho_q(\mathbf{x})\,\rho_q(\mathbf{y})}{|\mathbf{x}-\mathbf{y}|}\,, \tag{45}$$

where the self-energy is a constant for a rigid body at fixed position (contributing only a phase).

6.5 Derivation of the constrained influence functional

With the constraint solved, the gravitational degrees of freedom reduce to the coherent states $|\Phi_A\rangle$ attached to each matter branch. Tracing over the final gravitational field configuration yields the influence functional in three steps: a pure phase from the action difference, an overlap factor from the trace, and their product.

6.5.1 Step 1: The action difference gives a pure phase

For the superposition with $q^+(t) = \mathbf{x}_L$ and $q^-(t) = \mathbf{x}_R$ (static paths), the action difference is

$$S_{\text{eff}}[L] - S_{\text{eff}}[R] = -E_G\, t\,, \tag{46}$$

where

$$E_G \equiv \frac{GM^2}{d} \tag{47}$$

is the gravitational self-energy difference between the two configurations. This action difference produces a pure phase factor $e^{iE_G t/\hbar}$ in the off-diagonal density matrix element, which does not produce decoherence.

6.5.2 Step 2: The overlap factor

Decoherence arises from the trace over the final gravitational field state. The field in branch A is the constraint-determined coherent state $|\Phi_A(t)\rangle$, and the trace yields the overlap factor

$$\mathcal{O}(L,R;t) = \int dh_f\;\langle\Phi_L(t)|h_f\rangle\langle h_f|\Phi_R(t)\rangle = \langle\Phi_L(t)|\Phi_R(t)\rangle\;. \tag{48}$$

the inner product of the two coherent states—the quantum-mechanical distinguishability of the gravitational field configurations of the left and right branches.

6.5.3 Step 3: The constrained influence functional

Combining the phase and the overlap gives the constrained influence functional for the off-diagonal density matrix element.

Constrained influence functional.

For a mass M in spatial superposition (separation d), the influence functional obtained by imposing the linearized Wheeler-DeWitt constraint on the Schwinger-Keldysh path integral is

$$\mathcal{F}_{\text{constr}}[L, R;\, t] = \exp\Big(\frac{iE_G t}{\hbar}\Big) \;\times\; \langle \Phi_L(t) | \Phi_R(t) \rangle \;, \tag{49}$$

where $E_G = GM^2/d$ is the gravitational self-energy difference and $|\Phi_A(t)\rangle$ is the coherent state of the gravitational field determined by the constraint in branch A. The first factor is a pure phase that produces no decoherence. All decoherence resides in the second factor—the coherent-state overlap.

The reduced density matrix evolves as

$$\rho_{LR}(t) = \frac{1}{2}\, e^{iE_G t/\hbar}\; \langle \Phi_L(t) | \Phi_R(t) \rangle \;, \tag{50}$$

and the decoherence is measured by the decay of $|\rho_{LR}(t)|$, which is controlled entirely by the decoherence exponent:

$$\Gamma(t) = -\ln\big|\langle \Phi_L(t) | \Phi_R(t) \rangle\big|^2 \,. \tag{51}$$

6.6 G-counting: why the constrained result scales as G^1

The constrained influence functional (49) carries one power of G where the standard Feynman-Vernon result carries two; explicit power counting locates the missing power in the absent graviton propagator.

6.6.1 Standard FV: G^2 from the noise kernel

In the unconstrained calculation, the influence functional takes the noise-kernel form (cf. Section 5)

$$\mathcal{F}_{\text{FV}} = \exp\Big(-\frac{1}{\hbar^2}\int_0^t dt' \int_0^t dt''\; (\Delta q)^2\, \mathcal{N}(t' - t'')\Big) \,, \tag{52}$$

where $\mathcal{N}$ is the symmetrized noise kernel (Hadamard function) of the gravitational field. Each interaction vertex contributes a factor of $\sqrt{G}$ (from the matter-graviton coupling), and the noise kernel involves two such vertices, giving $(\sqrt{G})^2 = G$. However, the graviton propagator $\langle h\, h\rangle$ carries an additional factor of G (from the normalization of the graviton field: $h_{\mu\nu} \sim \sqrt{G}\,\hat{a}$), so the decoherence rate scales as

$$\Gamma_{\text{FV}} \sim \frac{1}{\hbar^2} \times G \times G \times (\text{matter}) = \frac{G^2 M^4}{\hbar^3 d^2} \,. \tag{53}$$

Both powers of G are unavoidable in the noise-kernel formalism: one from the coupling vertices, one from the propagator.

6.6.2 Constrained IF: G^1 from the coherent-state overlap

In the constrained case, decoherence is controlled by the overlap $|\langle\Phi_L|\Phi_R\rangle|$. The coherent-state overlap formula gives (Appendix G)

$$|\langle\Phi_L|\Phi_R\rangle|^2 = \exp\!\big(-\|\delta\alpha\|^2\big)\,, \tag{54}$$

where

$$\|\delta\alpha\|^2 = \int \frac{d^3k}{(2\pi)^3}\,|\alpha_L(\mathbf{k}) - \alpha_R(\mathbf{k})|^2\,. \tag{55}$$

From Eq. (40), the difference amplitude is

$$\delta\alpha(\mathbf{k}) \equiv \alpha_L(\mathbf{k}) - \alpha_R(\mathbf{k}) = -\frac{4\pi GM}{k^2}\cdot\frac{e^{-i\mathbf{k}\cdot\mathbf{x}_L} - e^{-i\mathbf{k}\cdot\mathbf{x}_R}}{\sqrt{2\hbar\omega_k}}\,. \tag{56}$$

The coherent-state amplitude obeys $\alpha \propto GM$, so $\delta\alpha \propto GM$ and $|\delta\alpha|^2 \propto G^2M^2$. The overlap exponent $\|\delta\alpha\|^2$ involves *no graviton propagator*—it is the norm of the amplitude in the single-particle Hilbert space, not a two-point correlation function. The mode integral gives

$$\|\delta\alpha\|^2 = \frac{(4\pi GM)^2}{2\hbar}\int\frac{d^3k}{(2\pi)^3}\,\frac{2(1-\cos\mathbf{k}\cdot\mathbf{d})}{k^4\,\omega_k} \;\propto\; \frac{GM^2}{\hbar\,c}\,\ln\!\Big(\frac{d}{\varepsilon}\Big)\,, \tag{57}$$

where the last step uses $\omega_k = ck$. The integral is IR-divergent (modes $k \lesssim 1/d$, regulated by the separation d) and UV-convergent at scale $k \sim 1/\varepsilon$ (ε the physical mass size); the dominant contribution comes from modes $1/d \lesssim k \lesssim 1/\varepsilon$, giving the logarithm $\ln(d/\varepsilon)$ (Appendix G). The result is dimensionless, as required for an exponent, and proportional to $GM^2/(\hbar c)$—one power of G, not two.

Proposition 6.1 (G^1 scaling of the constrained overlap)**.** *Within linearized gravity, the decoherence exponent of the constrained influence functional* (49) *scales as the first power of G,* $\Gamma \propto GM^2/(\hbar c)$*, in contrast to the* G^2 *scaling of the standard noise-kernel result* (53)*.*

Proof. In the standard FV approach one power of G comes from the matter-graviton vertices and a second from the graviton propagator $\langle h\,h\rangle$, which relates the field's quantum fluctuations to the coupling (Eq. (53)). Under the constraint the gravitational field does not fluctuate independently: it is locked to the matter by $\nabla^2\hat\Phi = 4\pi G\hat\rho$, and decoherence is governed by the distance between two coherent states in Hilbert space, $\|\delta\alpha\|^2$, rather than by the amplitude of vacuum fluctuations. By Eq. (57) this norm carries no propagator factor and evaluates to $\|\delta\alpha\|^2 \propto (GM^2/\hbar c)\,\ln(d/\varepsilon)$, a single power of G. □

6.7 Comparison with the standard influence functional

Table 1 summarizes the structural differences between the standard and constrained influence functionals.

The two calculations differ not by approximation—both are internally consistent within their frameworks—but in the *question they answer*:

- The standard FV calculation asks: starting from an undressed mass in the graviton vacuum, at what rate does dynamical graviton exchange generate entanglement between matter

Table 1. *Comparison of the standard and constrained influence functionals.*

	Standard FV	**Constrained IF**
Initial state	Product: $\lvert\psi\rangle\otimes\lvert 0\rangle$	Entangled: $(\lvert L\rangle\lvert\Phi_L\rangle + \lvert R\rangle\lvert\Phi_R\rangle)/\sqrt{2}$
Field at $t=0$	Same in both branches (vacuum)	Different in each branch (coherent)
Constraint	Not imposed	$\nabla^2\hat{\Phi} = 4\pi G\hat{\rho}$ enforced
Decoherence mechanism	Noise kernel $\mathcal{N}(t'-t'')$: dynamical entanglement generation	Coherent-state overlap $\langle\Phi_L\vert\Phi_R\rangle$: distinguishability of constraint-determined fields
G-scaling	G^2 (two vertices + propagator)	G^1 (overlap norm, no propagator)
d-scaling	$\Gamma \propto d^{-2}$	$\Gamma \propto d^{-1}$
Physical question	Rate of entanglement *generation*	Rate of entanglement *manifestation*
$\tau_{\rm dec}$ ($1\,\mu$g, $1\,$mm)	$\sim 10^{18}$ years	~ 1.6 ns

and field? The answer involves two interaction vertices (one emission, one absorption), hence two powers of the coupling $\sqrt{G}$, giving $\Gamma \propto G^2$.

- The constrained calculation asks: given that the Hamiltonian constraint has already entangled the mass with its gravitational field (a physical requirement, not an approximation), at what rate does this pre-existing entanglement produce operational decoherence? The answer involves the *distinguishability* of two coherent states, which depends on the norm $\|\delta\alpha\|^2$—a single power of G in the decoherence exponent.

Remark 6.2 (One overlap, two behaviours)*.* The generation/manifestation distinction is realized exactly in a solvable independent-boson model with the Hamiltonian constraint imposed. A single object—the branch overlap—yields both behaviours, selected only by the initial data. The unconstrained product state must *generate* branch distinguishability dynamically: its overlap decays through the noise (dissipative) part of the influence phase, at fourth order in the coupling ($\propto G^2$). The constrained state carries its distinguishability *statically*: the dressings are distinguishable from the outset, the modulus of the dressed overlap undergoes no dynamical decay, and the branch-energy (reactive) part of the influence phase is a reversible rotation at the dressing-energy scale—not, by itself, decoherence. Converting that reversible phase into an irreversible rate is precisely the relational step Axiom III makes—physical time read from the modular flow—and it is physically motivated rather than delivered by the model. The constrained Newtonian sector moreover carries no inter-branch field fluctuation (the field is slaved to the matter by the constraint), so for the physical state the dissipative channel vanishes identically and the rate is informational—set by the distinguishability of the dressings, not by noise. The transfer of this mechanism to full gravity carries the same conjectural status as the operator identity of Section 7.3.

6.7.1 Why gravity is special

The analogous argument fails for QED, where Gauss's law $\nabla\cdot\hat{\mathbf{E}} = \hat{\rho}_e/\epsilon_0$ also constrains the field. At the level of the *overlap computation* (Sections 6.2–6.6) the two cases are structurally similar: a charged particle in superposition is dressed by branch-dependent coherent states of the longitudinal electric field, and the overlap $\langle E_L\rangle\, E_R$ is less than unity.

The difference emerges at *rate extraction* (Section 7.3). In QED, time is a background parameter and the Hamiltonian H_{QED} is unconstrained: unitary evolution preserves the overlap $|\langle E_L(t)\rangle\, E_R(t)|$, producing a reversible phase oscillation [30]. In gravity, the Wheeler-DeWitt constraint $\hat{H}_{\mathrm{total}} = 0$ eliminates background time; physical time emerges from internal correlations (the Page-Wootters mechanism [31]), and the irreducible quantum uncertainty of this gravitational clock converts the overlap reduction into irreversible decoherence. In the algebraic formulation, the Hamiltonian constraint converts the Type III observable algebra to Type II, introducing a finite trace and spectral gap that sets the decoherence rate [12, 13]; Gauss's law restricts the state space but does not change the algebra type.

Remark 6.3 (Scope of the gravity/QED distinction)*.* This distinction is fully operative only in the *complete* (nonlinear) quantum gravity theory. In the linearized limit used for the explicit computations of this paper, the Hamiltonian constraint reduces to the Poisson equation $\nabla^2\Phi = 4\pi G\rho$, which has the same *spatial* form as Gauss's law. The rate extraction in Section 7.3 therefore invokes the full WDW structure—specifically, the modular Hamiltonian identification (68) and the Page-Wootters mechanism—within a linearized calculation that is consistent with (and controlled by) the full theory. A fully nonlinear derivation that makes the gravity/QED distinction manifest at each step remains an open problem.

Remark 6.4 (Validity)*.* The derivation is valid within linearized gravity, with expansion parameter $GM/(c^2 d) \sim 7\times 10^{-34}$ for laboratory parameters ($M = 1\ \mu$g, $d = 1\,$mm). All higher-order corrections—graviton self-interaction, pair production, backreaction, and renormalization of G—are suppressed by at least $O\big((GM/(c^2 d))^2\big) \sim 5\times 10^{-67}$ relative to the leading term (Appendix H). The result (49) is exact at $O(G)$.

7 The Decoherence Rate

Evaluating the constrained influence functional of Section 6 yields a decoherence rate scaling as G^1, not G^2, with the gravitational self-energy $E_G = GM^2/d$ setting the scale.

7.1 Evaluating the coherent-state overlap

In the constrained framework the decoherence factor is the overlap of two time-dependent coherent states of the gravitational field, one per branch of the matter superposition. For $t < 0$ the mass is localized and the field occupies a single constraint-satisfying coherent state $|\Phi_0\rangle$. At $t = 0$ a beam splitter places the mass in $(|L\rangle + |R\rangle)/\sqrt{2}$; the constraint demands two distinct coherent states $|\Phi_L\rangle$ and $|\Phi_R\rangle$, but the field adjusts at the speed of light, so the *difference field* builds up causally from zero by the driven-oscillator solution (Appendix G). The common-mode field $(\alpha_L + \alpha_R)/2$ remains equal to α_0 and drops out. The difference-field mode amplitude at time t is

$$\alpha_A(\mathbf{k}, t) \;=\; \alpha_A^{\mathrm{eq}}(\mathbf{k})\left(1 - e^{-i\omega_k t}\right), \tag{58}$$

where $\omega_k = c|\mathbf{k}|$ and the equilibrium amplitude is determined by the Newtonian potential of a point mass at position $\mathbf{x}_A$:

$$\alpha_A^{\mathrm{eq}}(\mathbf{k}) \;=\; -\frac{4\pi GM}{k^2}\,\frac{e^{-i\mathbf{k}\cdot\mathbf{x}_A}}{\sqrt{2\hbar\omega_k}}\,. \tag{59}$$

At each instant the gravitational field state in branch A is the coherent state $|\Phi_A(t)\rangle = D\big(\alpha_A(\cdot,t)\big)\,|0\rangle$, where D is the multimode displacement operator.

The squared overlap of the two branch states is

$$\big|\langle\Phi_L(t)\rangle\,\Phi_R(t)\big|^2 \;=\; \exp\!\Big(-\int \frac{d^3k}{(2\pi)^3}\,\big|\alpha_L(\mathbf{k},t)-\alpha_R(\mathbf{k},t)\big|^2\Big)\,, \tag{60}$$

a standard identity for coherent states. The difference amplitude factorizes:

$$\alpha_L(\mathbf{k},t)-\alpha_R(\mathbf{k},t) \;=\; \delta\alpha(\mathbf{k})\,\big(1-e^{-i\omega_k t}\big)\,, \tag{61}$$

where the *equilibrium difference*

$$\delta\alpha(\mathbf{k}) \;=\; -\frac{4\pi GM}{k^2}\,\frac{e^{-i\mathbf{k}\cdot\mathbf{x}_L}-e^{-i\mathbf{k}\cdot\mathbf{x}_R}}{\sqrt{2\hbar\omega_k}} \tag{62}$$

encodes the spatial information of the superposition.

7.2 The decoherence exponent

Inserting Eqs. (61) and (62) into (60) and writing $|1-e^{-i\omega_k t}|^2 = 2(1-\cos\omega_k t)$, we obtain

$$\Gamma(t) \;\equiv\; -\ln\big|\langle\Phi_L(t)\rangle\,\Phi_R(t)\big|^2 \;=\; \int \frac{d^3k}{(2\pi)^3}\,\big|\delta\alpha(\mathbf{k})\big|^2\,2\big(1-\cos\omega_k t\big)\,. \tag{63}$$

exact within linearized gravity with a free graviton field; the matter decoherence is determined entirely by this integral.

The squared difference amplitude is

$$\big|\delta\alpha(\mathbf{k})\big|^2 \;=\; \frac{(4\pi GM)^2}{k^4}\,\frac{1}{2\hbar\omega_k}\,2\big(1-\cos\mathbf{k}\cdot\mathbf{d}\big)\,, \tag{64}$$

where $\mathbf{d}=\mathbf{x}_L-\mathbf{x}_R$ is the separation vector. Substituting into (63), converting to spherical coordinates, and performing the angular integral yields

$$\Gamma(t) \;=\; \frac{16G^2M^2}{\pi\hbar c}\int_0^{\Lambda}\frac{dk}{k^3}\,\Big(1-\frac{\sin kd}{kd}\Big)\,\big(1-\cos ckt\big)\,, \tag{65}$$

with Λ a UV cutoff that drops out of the rate. Two time regimes follow.

Short times ($t \ll d/c$). Expanding $1-\cos ckt \approx (ckt)^2/2$ gives quadratic growth $\Gamma(t)\propto t^2$: Gaussian (non-Markovian) decay—the quantum Zeno regime.

Long times ($t \gg d/c$). Modes with $k \lesssim 1/d$ have completed many oscillations and contribute their time-averaged value $\langle 2(1-\cos\omega_k t)\rangle \to 2$, so $\Gamma(t)$ approaches the static overlap $\|\delta\alpha\|^2$ of the two equilibrium coherent states. The rate of approach to this equilibrium is the decoherence rate, governed by the time derivative

$$\frac{d\Gamma}{dt} \;=\; 2\int\frac{d^3k}{(2\pi)^3}\,\big|\delta\alpha(\mathbf{k})\big|^2\,\omega_k\,\sin\omega_k t\,. \tag{66}$$

For t in the window $d/c \ll t \ll t_{\rm eq}$ (after light-crossing but before full equilibration) this rate is effectively constant and equal to the Diósi-Penrose rate, established below through the constraint mechanism.

7.3 From energy scale to rate: the role of the Hamiltonian constraint

The free-field mode integral (65) establishes the decoherence *energy scale* $E_G = GM^2/d$, scaling as G^1. Treated as a free-field overlap, however, the exponent $\Gamma(t)$ *saturates* at the equilibrium value $2\|\delta\alpha\|^2$ rather than growing linearly in t (Appendix G): each mode contributes a bounded factor $2(1 - \cos\omega_k t)$, and the integral converges to a finite constant by the Riemann-Lebesgue lemma. The saturation is structural, not an artifact of the vacuum state: in frequency space the free graviton bath seen by the which-path coordinate is *super-Ohmic*—its spectral density vanishes as ω^3 at low frequency—and a super-Ohmic bath has no zero-frequency weight to sustain a Markovian rate at any temperature.

Extraction of a decoherence *rate* $\Gamma = E_G/\hbar$ (linear growth in t) requires physical input beyond the free-field overlap, supplied by the Hamiltonian constraint. The linearized Wheeler-DeWitt constraint

$$(\hat{H}_{\rm matter} + \hat{H}_{\rm grav})\,|\Psi_{\rm phys}\rangle = 0 \tag{67}$$

is not merely a condition on the initial state; it is enforced at *all times*. This has three interrelated consequences:

1. **No independent graviton dynamics.** The constraint continuously slaves the gravitational field to the matter configuration. The gravitational field does not propagate as an independent degree of freedom—its state is determined, mode by mode, by the matter distribution. This replaces the free graviton propagator (which costs one power of G in perturbation theory) with a constraint-determined classical field (which costs zero additional powers of G).

2. **Physical time from the constraint.** Since $H_{\rm total} = 0$, the physical state is "timeless." Physical time emerges relationally: the matter system evolves with respect to the gravitational field as an internal clock (the Page-Wootters mechanism [31]). The rate of decoherence is set by the energy gap between the two constraint-satisfying branches, which is the gravitational self-energy $E_G = GM^2/d$.

3. **Modular Hamiltonian identification.** The Bisognano-Wichmann theorem [32] identifies the vacuum modular Hamiltonian K_0 with 2π times the boost generator. For coherent-state perturbations of the gravitational field, the Baker-Campbell-Hausdorff expansion of the free-field modular algebra terminates at linear order, and the bi-local correction $\delta K_{\rm nonlocal}$ vanishes in expectation values and in the solvable models we test (Sec. 9), so the full modular Hamiltonian satisfies [33]

$$K = 2\pi H_{\rm phys} + O(G^2) \tag{68}$$

We adopt (68) as an operator equation on the physical Hilbert space; at the full operator level it is a conjecture—established here in expectation values and in solvable models, and reducing to the construction of the crossed-product algebra for a finite causal diamond

Mechanism	G-counting	Result
Standard Feynman-Vernon		
Two interaction vertices	$\sqrt{G} \times \sqrt{G} = G$	
Graviton propagator	$\times\, G^0$ (free propagator)	
Noise kernel ($\langle H_{\rm int}^2 \rangle$)	$= G^2$	$\Gamma \sim G^2 M^4/(\hbar^3 d^2)$
Constrained Feynman-Vernon		
Gravitational self-energy	$E_G = GM^2/d$	
No propagator needed	(constraint-determined field)	
Single energy insertion	$= G^1$	$\Gamma = GM^2/(\hbar d)$

Table 2. *G-counting comparison. In the standard influence functional, the noise kernel involves two interaction vertices, each contributing $\sqrt{G}$, yielding G^2 overall. In the constrained influence functional, the Hamiltonian constraint replaces the graviton propagator with a constraint-determined classical field, removing one power of G. The decoherence rate is set by the gravitational self-energy $E_G \sim G^1$.*

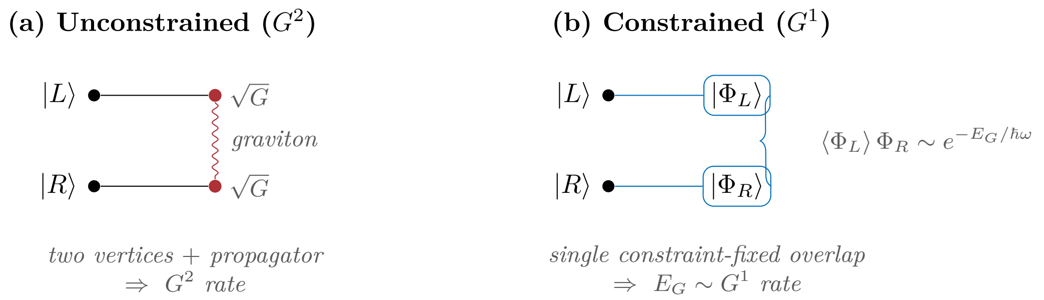

Figure 1. *Schematic diagrams for the two decoherence mechanisms. **(a)** In the standard influence functional, decoherence proceeds through graviton exchange between branches, giving G^2. **(b)** In the constrained influence functional, each branch carries a coherent state determined by the constraint; decoherence is the overlap of these states, giving G^1.*

(Sec. 9). Decoherence proceeds at the modular frequency $\omega_{\rm mod} = \Delta K/\hbar = 2\pi E_G/\hbar$, yielding

$$\Gamma = \frac{E_G}{\hbar} = \frac{GM^2}{\hbar d}\,. \tag{69}$$

The G-counting is summarized in Table 2.

7.4 Diagrammatic picture

The G-counting admits a diagrammatic interpretation (Fig. 1).

In the *unconstrained* (perturbative) calculation, decoherence arises from a graviton-exchange loop: one interaction vertex on the left branch ($\sqrt{G}$), one on the right ($\sqrt{G}$), connected by a free graviton propagator (G^0). Squaring the amplitude gives the double-commutator noise kernel, scaling as $(\sqrt{G})^2 \times (\sqrt{G})^2 = G^2$.

In the *constrained* calculation there is no graviton propagator: each branch carries a constraint-determined coherent state, and decoherence is the overlap of the two—a single constraint insertion contributing $E_G \sim G^1$. The loop opens into a tree, the graviton line a background field fixed by the constraint rather than a propagator.

7.5 The $O(1)$ coefficient

The G-counting fixes the decoherence rate up to an $O(1)$ prefactor C in $\Gamma_{\rm dec} = C\,E_{\rm G}/\hbar$. Three independent considerations constrain this coefficient, and together they bound it to the narrow window $C \in [2/\pi,\, 1]$ set by the Margolus–Levitin quantum speed limit.

(i) Margolus–Levitin floor. Decoherence requires the two branch states of the gravitational field to become distinguishable—to evolve toward orthogonality. The Margolus–Levitin theorem bounds the rate at which a system with mean energy $E_{\rm G}$ above its ground state can reach an orthogonal state by $\Gamma_{\rm ML} = 2E_{\rm G}/(\pi\hbar)$ (derived in Appendix I). Identifying $E_{\rm G} = GM^2/d$ as the energy driving the orthogonalization, this is the slowest admissible distinguishing rate and corresponds to the coefficient floor $C = 2/\pi \approx 0.637$. The Diósi–Penrose rate $\Gamma_{\rm DP} = E_{\rm G}/\hbar$ lies a factor $\Gamma_{\rm DP}/\Gamma_{\rm ML} = \pi/2 \approx 1.57$ above this floor, i.e. at $C = 1$. The two differ only by an order-unity factor—in sharp contrast to the perturbative G^2 rate, which lies a factor $\sim (M/M_{\rm P})^2(\ell_{\rm P}/d) \sim 10^{-35}$ *below* $\Gamma_{\rm ML}$ for laboratory masses (Appendix I). This places the physical G^1 rate at the fundamental information-theoretic scale, and bounds C from below.

(ii) Mode counting. The coherent-state overlap computation (Appendix G) evaluates (63) in the Newtonian limit and yields $C = 1$ when the self-energy divergences are renormalized by subtracting the single-branch contributions. The resulting rate matches the Diósi master equation [5, 34], in which the decoherence kernel is

$$\mathcal{D}[\rho] \;=\; -\frac{G}{\hbar}\int d^3x\, d^3y\; \frac{[\hat\rho(\mathbf{x}),\, [\hat\rho(\mathbf{y}),\, \rho]]}{|\mathbf{x}-\mathbf{y}|}\,. \tag{70}$$

This Lindblad generator produces a decoherence rate for a point-mass superposition of exactly $\Gamma = GM^2/(\hbar d)$.

(iii) Constraint identification and modular flow. The Diósi noise kernel $G/|\mathbf{x}-\mathbf{y}|$ is *not* an independent postulate: it is the Green function of the Poisson constraint $\nabla^2\Phi = 4\pi G\rho$. This identification connects the noise kernel directly to the Hamiltonian constraint, giving a first-principles origin for the Diósi master equation, and the identification (68) relates the modular frequency to the physical energy gap. Both point to $C = 1$ for the most natural choice—a static observer at the location of the mass, with Markovian dephasing.

The window's two edges are not competing estimates of one number; they are two *observables*. The coefficient $C = 1$ is the decay rate of the continuous interferometric visibility (Markovian dephasing, the quantity an interference experiment measures); $C = 2/\pi$ is the discrete Margolus–Levitin orthogonalization tick (the earliest time at which the branch dressings can reach a perpendicular state). Conditional on the modular identification (68), the visibility coefficient is $C = 1$ exactly; the residual window records the choice of observable and the conjectural status of that identification.

Combining these considerations, the best determination is $C = 1$ (Markovian dephasing, matching the Diósi master equation, and the coefficient interferometry measures), bounded below by the Margolus–Levitin floor $C = 2/\pi$, so $C \in [2/\pi,\, 1] \approx [0.637,\, 1.000]$. The uncertainty resides in the $O(1)$ prefactor only; the G^1 scaling is robust. The main result is:

$$\Gamma_{\text{dec}} = C \times \frac{GM^2}{\hbar d} + \mathcal{O}(G^2), \qquad C \in [2/\pi,\, 1] \tag{71}$$

For $C = 1$ (matching the Diósi master equation), a particle of mass $M = 1\ \mu$g in a superposition of separation $d = 1$ mm has

$$\tau_{\text{dec}} = \frac{\hbar d}{GM^2} = \frac{(1.055 \times 10^{-34}\ \text{J s})(10^{-3}\ \text{m})}{(6.674 \times 10^{-11}\ \text{m}^3\,\text{kg}^{-1}\,\text{s}^{-2})(10^{-9}\ \text{kg})^2} \approx 1.58\ \text{ns}\,. \tag{72}$$

This prediction is $\sim 10^{34}$ times shorter than the perturbative G^2 estimate (35) and lies within the sensitivity window of planned experiments (Section 8).

7.6 Validity of the derivation

The result (71) rests on linearized gravity, where the gravitational field is treated as a free quantum field on a flat background sourced by a classical mass distribution. The expansion parameter is $GM/(c^2 d) \sim 7 \times 10^{-34}$ for the laboratory parameters above, so all $O(G^2)$ corrections are suppressed by $(GM/(c^2 d))^2 \sim 5 \times 10^{-67}$. In particular:

- *Graviton self-interactions*: contribute at $O(G^2)$ and are negligible.
- *Graviton pair production*: the squeezing parameter $r_{\text{sq}} \sim GM/(c^2 d) \sim 7 \times 10^{-34}$ is far too small to produce appreciable non-coherent excitations.
- *Backreaction*: the gravitational field energy $E_G = GM^2/d \sim 6.7 \times 10^{-26}$ J is negligible compared to the rest mass energy $Mc^2 \sim 10^{-10}$ J.
- *Running of G*: renormalization-group corrections to G are suppressed by $(E/E_{\text{Planck}})^2 \sim 10^{-76}$.

The linearized approximation is extraordinarily well controlled for all experimentally relevant parameter regimes. See Appendix H for a detailed analysis of each $O(G^2)$ correction.

Part III

Predictions and Discussion

8 Testable Predictions

The framework's predictions fall in three tiers by their standing within the theory: the core laboratory prediction, carried by the axioms; companion cosmological results, developed in the companion papers of this series; and Planck-scale phenomenology, a speculative ultraviolet extension. The table collects them with their sources and tests.

Prediction	Formula	Standing	Test
Grav. decoherence	$\tau = \hbar d/(GM^2)$	Core (Axiom III + WDW constraint)	Optomechanics
Dark energy	$\rho = \alpha H^2 c^2/G$	Companion (Axiom I + GSL)	DESI, Euclid
MOND scale	$a_0 = cH_0/(2\pi)$	Companion (Axiom II, de Sitter)	Rotation curves
Min. length	$\Delta x_{\min} \approx \sqrt{2}\,\ell_P$	Speculative UV extension	GUP bounds
Mod. dispersion	E^2 scaling	Speculative UV extension	GRB timing
Birefringence	E^3 scaling	Speculative UV extension	GRB polarimetry

8.1 Gravitational decoherence

The gravitational decoherence prediction (Part II) is the framework's core falsifiable content and the most accessible to near-term experiment. A particle of mass M in a spatial superposition of separation d has decoherence time $\tau_{\text{dec}} = \hbar d/(GM^2)$; for $M = 1$ μg and $d = 1$ mm this is approximately 1.6 ns, a regime levitated optomechanics is approaching. The benchmark is quoted in the point-mass convention of Section 4; for a physical sphere of the same mass the self-energy saturates at the particle radius and the rate is faster and separation-independent, as developed there and in the companion BMV paper. Detection at the predicted rate confirms Axioms I and III; non-detection falsifies the G^1 scaling central to the framework.

Four signatures jointly identify a gravitational origin and distinguish it from every known environmental mechanism (Section 7):

1. **Mass scaling** $\Gamma \propto M^2$ ($\tau \propto M^{-2}$): doubling the mass quadruples the rate. Environmental mechanisms scale differently—photon scattering as $M^{2/3}$ for constant-density particles, collisional decoherence linearly in M.

2. **Temperature independence**: $E_{\text{G}} = GM^2/d$ depends only on the mass configuration, not on the thermal state. Unlike thermal decoherence, the rate persists as $T \to 0$.

3. **Vacuum independence**: gravitational decoherence cannot be shielded and survives in the most perfect vacuum, whereas collisional and photon-scattering channels are suppressed by improving the vacuum.

4. **Linear separation scaling** $\Gamma \propto 1/d$ ($\tau \propto d$): doubling the separation halves the rate—the opposite of most environmental mechanisms (and of the perturbative G^2 prediction, where $\Gamma \propto 1/d^2$). This counterintuitive inverse scaling is a direct consequence of $E_{\text{G}} = GM^2/d$ in the point-mass regime.

No known mechanism exhibits all four simultaneously; their joint observation is a unique fingerprint. The G^1 and G^2 predictions differ by $(M_{\text{P}}/M)^2(d/\ell_{\text{P}}) \approx 3 \times 10^{34}$ at the 1 μg, 1 mm benchmark, so even an order-of-magnitude measurement discriminates between them, with no precise determination of the $\mathcal{O}(1)$ coefficient required.

8.2 Companion cosmological predictions

Applied to the cosmological horizon, the same axioms yield the holographic dark energy density $\rho_{\text{DE}} = \alpha H^2 c^2/G$ with $\alpha \approx 0.082$ and equation of state $w = -1$ exactly, with no time evolution [7]; any statistically significant detection of $w \neq -1$ by DESI or Euclid falsifies the mechanism as formulated. The entanglement-equilibrium dynamics of Axiom II, applied to de Sitter thermodynamics, reproduce the MOND acceleration scale $a_0 = cH_0/(2\pi) \approx 1.08 \times 10^{-10}$ m/s^2 with no free parameters. Both results are derived and defended in the companion papers; we list them here because they test the same three axioms in a regime sixty orders of magnitude from the laboratory one.

8.3 Planck-scale phenomenology (speculative)

The minimum length, modified dispersion, and vacuum birefringence of Section 3 are speculative ultraviolet extensions, not axiom consequences. Their value is discriminatory: the E^2 dispersion scaling and E^3 birefringence scaling differ from the E^1 and E^2 signatures of alternative frameworks (loop-quantum-gravity scenarios, Myers–Pospelov, the Standard Model Extension), and the dispersion coefficient equals the GUP coefficient ($\xi = \beta_{\mathrm{GUP}}$ by construction), a correlation between independently measurable quantities that would evidence their common origin.

8.4 Falsification criteria

Prediction	**Falsified if**	**Axioms tested**
$\tau_{\mathrm{dec}} = \hbar d/(GM^2)$	No decoherence at G^1 rate	I + III
$w = -1$ (exact)	$w \neq -1$ at any z by $> 3\sigma$	I
$\Delta x_{\mathrm{min}} = \sqrt{2}\,\ell_P$	$\beta_{\mathrm{GUP}} < 0.1$ or $\beta_{\mathrm{GUP}} > 10$	UV ext.
E^2 dispersion scaling	$\xi < 0.01$ from GRB timing	UV ext.
E^3 birefringence	Achromatic polarization	UV ext.

The framework is falsifiable at every tier, and the tiers are ordered by commitment: the decoherence row tests the axioms themselves; the cosmology rows test their application to horizons; the remaining rows test an extension the axioms do not require.

9 Discussion

The framework offers a unified axiomatic foundation for quantum-gravitational phenomena, with its sharpest concrete consequence the G^1-rate gravitational decoherence. This section assesses limitations, relates the framework to alternative approaches and prior decoherence proposals, and identifies the most promising experimental tests.

9.1 Unification across scales

The framework makes predictions at the Planck scale ($\ell_{\mathrm{P}} \sim 10^{-35}$ m: minimum length and GUP), laboratory scales (μm–mm: gravitational decoherence), astrophysical scales (modified dispersion and birefringence), and cosmological scales (Gpc $\sim 10^{26}$ m: holographic dark energy)—roughly sixty orders of magnitude. Three primitive axioms generate consistent predictions across this range by operating at their natural scales: modular time and gravitational decoherence at laboratory scales, horizon entropy at cosmological scales, and—as a speculative ultraviolet extension—generalized-uncertainty estimates at the Planck scale. The same physics manifests differently by observational regime: matter–geometry entanglement accumulates rapidly for massive objects, so gravitational decoherence dominates at laboratory scales; horizon areas become cosmologically significant, so holographic bounds dominate at cosmological scales;

modified commutation relations become non-negligible, so Planck-scale effects dominate at high energies. All emerge from the same axioms and their derived Semiclassical Duality Correspondence.

The same axioms underlie the companion results that we do not develop here. Applied to a cosmological horizon, the Holographic Bound (Theorem 2.6) and Generalized Entropy (Axiom I) yield a holographic dark energy density $\rho_{\mathrm{DE}} = \alpha c^2 H^2/G$ with $\alpha \approx 0.082$ and equation of state $w = -1$ [7]; the entropic dynamics of Axiom II, applied to de Sitter thermodynamics, reproduce the MOND acceleration scale $a_0 = cH_0/(2\pi) \approx 1.08 \times 10^{-10}$ m/s^2 with no free parameters. We cite these connections to locate the present paper within the series, not to re-derive them.

9.2 The decoherence mechanism: interpretation and prior work

The gravitational decoherence developed in Part II bridges the phenomenological Diósi–Penrose formula and the perturbative QFT result. Diósi [5] *postulated* a stochastic gravitational noise field whose correlation kernel is the Newtonian potential $1/|\mathbf{x} - \mathbf{y}|$, leading to a Lindblad master equation with rate $GM^2/(\hbar d)$. Section 6 shows that this kernel is not an independent postulate: it is the Green function of the Poisson constraint $\nabla^2\Phi = 4\pi G\rho$, so the Diósi master equation follows from the Wheeler–DeWitt constraint. Penrose [6] argued on heuristic grounds that superpositions of distinct geometries should decay on a timescale $\hbar/E_{\mathrm{G}}$; our coherent-state-overlap mechanism supplies the microscopic content behind that argument. Anastopoulos and Hu [25] and Blencowe [26] performed the careful perturbative calculation that gives G^2; their result is correct for the unconstrained product state, and the present work does not invalidate it but changes the starting point.

These authors differ in *interpretation* as much as in mechanism. Penrose's objective-reduction reading treats gravity as causing genuine wave-function collapse; the present reading treats the gravitational degrees of freedom as an environment, so that tracing over them produces effective collapse while the global state stays pure and unitary. All G^1 models make the same parametric prediction $\tau_{\mathrm{dec}} \propto \hbar d/(GM^2)$; they differ in interpretation rather than quantitative content. Distinguishing them would require measuring the entropy of the combined system-plus-environment—demonstrating either that it increases (genuine collapse) or stays constant (unitary evolution)—which is extraordinarily challenging. The mass scaling, however, already discriminates against alternatives of different parametric form: Károlyházy's spacetime-uncertainty model [35] predicts $\tau \propto M^{-1}$ rather than M^{-2}.

9.3 Why gravity, and not electromagnetism

A natural objection is that electromagnetism has an analogous constraint—Gauss's law likewise dresses a charged particle with a branch-dependent coherent state of its Coulomb field, and the overlap computation is structurally identical through Section 6. The two theories part at rate extraction, as developed there: Gauss's law is a spatial constraint that restricts the state space but leaves time a background parameter and the algebra type unchanged, whereas the Hamiltonian constraint eliminates background time and converts the Type III observable algebra to Type II with a finite trace. The criterion is compact: a first-order rate exists precisely where the constraint identifies modular flow with time evolution. Gravity satisfies the criterion (conjecturally, at the operator level); electromagnetism demonstrably does not; the corresponding experimental statement—a charged and a neutral particle of equal mass decohere gravitationally at the same rate—is itself testable.

9.4 Limitations

Six limitations must be acknowledged honestly.

First, the axioms determine scaling behaviour but not numerical coefficients. The GUP parameter $\beta_{\rm GUP}$ is predicted to be of order unity (best estimate $\beta_{\rm GUP} = 2$, range 1–4); the sign of the dispersion coefficient ξ is not fixed by the axioms. Likewise, the decoherence rate is fixed only up to the $\mathcal{O}(1)$ coefficient C in $\Gamma_{\rm dec} = C\, E_{\rm G}/\hbar$. The Margolus–Levitin bound narrows this to $C \in [2/\pi, 1]$ (Section 7 and Appendix I), with natural value $C = 1$ and floor $C = 2/\pi$, but does not pin it uniquely; experiments should primarily test the scaling relations ($\tau \propto M^{-2}$, $\tau \propto d$, $\Gamma \propto G^1$) rather than the absolute coefficient.

Second, the entanglement-geometry content of Axiom I generalizes results established in AdS/CFT to arbitrary spacetimes. This generalization is well-motivated—the Ryu–Takayanagi formula and its extensions suggest a deep entanglement–geometry connection that should not depend on the specific features of anti-de Sitter space—but a rigorous derivation for general spacetimes remains open. The axiom should be regarded as a conjecture supported by strong evidence, not a proven theorem.

Third, the framework provides no ultraviolet completion. The axioms describe the semiclassical regime, where matter is quantum but geometry can be treated classically or semiclassically. At the Planck scale itself the framework breaks down; a complete theory of quantum gravity would describe that regime. This limitation is shared by essentially all current approaches to quantum-gravity phenomenology.

Fourth, the Born rule is assumed throughout but not derived. Decoherence—whether environmental or gravitational—explains why interference terms between macroscopically distinct states become unobservable, but it does not by itself explain why measurement outcomes are definite, nor why their probabilities take the Born-rule values. This is a foundational gap shared with essentially all formulations of quantum mechanics.

Fifth, the G^1 scaling deserves special comment. It is *derived in linearized gravity within a controlled approximation* by imposing the Wheeler–DeWitt constraint—the single physical input that carries the derivation—with four further convergent lines of motivation (Appendix F). The energy-scale identification ($E_{\rm G} = GM^2/d$, a single power of G) is rigorous within linearized gravity; the extraction of a *rate* from this energy scale invokes the Hamiltonian constraint and the Page–Wootters mechanism, and is the less rigorous step. Standard perturbative QFT gives G^2 and is correct for its (unconstrained) product state. The two calculations answer different questions—entanglement *generation* from an unphysical product state (G^2) versus *manifestation* of constraint-enforced entanglement (G^1). The central relation $K = 2\pi H_{\rm phys} + \mathcal{O}(G^2)$ (Eq. 68) is on the same footing: we establish it at the level of expectation values and in solvable models (where the bi-local correction $\delta K_{\rm nonlocal}$ is verified to vanish), but its validity as a *full operator identity* on the physical Hilbert space remains a conjecture. For conformally invariant matter the corresponding identity is rigorous—the global Hamiltonian is reconstructible from the vacuum modular Hamiltonian of a ball, with $K_H = 2\pi H$, and the departure for non-conformal matter is controlled, entering at the order fixed by the relevant coupling [36]. The open case is the gravitational (constraint-sector) realization, where the obstruction is sharply localized: the displacement that transports the vacuum modular Hamiltonian to the matter-loaded sector has support outside the wedge, and the Type III_1 algebra of the flat-space wedge admits no tensor split. Two considerations temper the obstruction. First, the flat-space setting is itself an idealization: for any positive cosmological constant the observer's causal patch carries a Type II algebra with a canonical trace as a theorem, the modular identification holds for the static patch, and the laboratory rate is recovered as the controlled $H \to 0$ limit—at the observed value of H the de Sitter correction to the benchmark rate is negligible to dozens of digits. Second, the decoherence-relevant quantity is the *difference* between the two branch dressings, a dipole field two powers more localized than either branch's monopole, so the outside-wedge support that drives the obstruction is doubly suppressed for laboratory geometries. The question nonetheless reduces to a single well-posed construction—the crossed-product (Type II) algebra for a finite causal diamond with conformal-Killing flow—whose resolution would simultaneously legitimize the operator identity, the rate extraction, and the coefficient $C = 1$; the companion papers on graviton modular flow and on the quantitative obstruction bound develop it. Ultimately the scaling is an empirical question, and the framework makes a falsifiable prediction.

Sixth, some predictions of the framework—gravitational decoherence, holographic dark energy—also appear in prior work. The contribution here is not to discover these effects but to unify them within a common axiomatic structure and to derive additional predictions (GUP, modified dispersion, birefringence) from the same principles.

9.5 Relation to other approaches

Quantum-Geometric Correspondence is not a replacement for string theory, loop quantum gravity, asymptotic safety, or causal set theory, but a complementary phenomenological perspective: it takes quantum-gravitational effects as given and systematizes their relationships through axioms. A microscopic theory of quantum gravity may eventually derive these axioms from deeper principles, much as statistical mechanics underlies thermodynamics.

The central mechanism here—that imposing the Hamiltonian (Wheeler–DeWitt) constraint forces an entangled gravity–matter state—has an independent and closely related realization in recent work: Long and Zhang [37] show that the Hamiltonian constraint of canonical quantum gravity generates gravity–matter entanglement in quantum field theory. Their result is mechanistically convergent with the constrained-influence-functional picture developed here and reached by a different route; we regard it as supporting, not superseding, the present derivation, whose specific contribution is the G^1 decoherence rate and its laboratory falsifiability.

9.6 Outlook

The decisive question is experimental, and it is the G^1 versus G^2 scaling of gravitational decoherence. Levitated optomechanics, matter-wave interferometry, and proposed space-based platforms are approaching the regime where the prediction becomes testable; a phased program—first testing the M^2 scaling law across accessible masses, then measuring absolute decoherence times—can progressively discriminate the two scenarios. If decoherence is observed at the G^1 rate, gravity has an irreducibly classical character at the quantum interface, and the framework receives strong confirmation; if it is observed at the G^2 rate or not at all, Axiom III (Modular Time) must be revised or abandoned. In parallel, $w = -1$ from DESI and Euclid, E^3 birefringence scaling from GRB polarimetry, and the coefficient correlation $\xi = \beta_{\mathrm{GUP}}$ from independent measurements provide additional tests of the framework.

In conclusion, the Quantum-Geometric Correspondence establishes matter–geometry entanglement in the semiclassical regime as a fundamental physical phenomenon. Three primitive axioms and their derived results yield a coherent chain from foundational principles to a falsifiable nanosecond-scale laboratory prediction carried by Axiom III (Modular Time), the framework's conjectural clause, and unify gravitational decoherence with holographic dark energy and emergent gravity within a common structure. Experiment will determine whether this unification corresponds to physical reality.

Appendices

A Logical Structure of the Axiom System

A primitive axiom must not be derivable from the others; a derivable statement is a theorem, not a primitive. The framework rests on three primitive axioms (I–III). The Observer-Dependent Horizon Principle (Theorem 2.5) and the Holographic Bound (Theorem 2.6) are derived results, hence excluded from the independence analysis. Independence of I–III is established by countermodels: frameworks satisfying the remaining axioms while violating the one under study.

Lemma A.1 (Countermodels prove independence)**.** *If Axiom n were derivable from the others, every model satisfying those would satisfy Axiom n. A model satisfying the rest but not n therefore witnesses, by contradiction, that Axiom n is independent.*

The countermodels are given in summary form; full construction requires specification of the underlying mathematical structures, indicated here only through the physical feature that violates each axiom.

A.1 Axiom I (Generalized Entropy)

Axiom I has two facets—global unitarity of the total (matter-plus-geometry) state, and identification of the geometric entropy with the Bekenstein–Hawking area term—and a countermodel need violate only one.

1. Semiclassical gravity formulated before the resolution of the information paradox violates the first. Matter falling into a black hole is absorbed; the hole evaporates via thermal Hawking radiation carrying no information about the infalling matter. The von Neumann entropy of the radiation exceeds that of the infalling matter, with no compensating geometric term once the hole has evaporated; information is lost.

2. JT gravity with logarithmic corrections violates the second: the entropy–area relation acquires $S \sim A/(4\ell_P^2) + c \ln A + \ldots$, breaking the proportionality.

Each construction satisfies the other axioms in appropriate limits.

A.2 Axiom II (Entanglement Equilibrium)

A gravity theory with the same generalized-entropy assignment but non-Einstein field equations is the countermodel—Jacobson's argument run in reverse. Take an $f(R)$ theory whose regions carry the area-form entropy of Axiom I; its small causal diamonds are *not* at entanglement equilibrium ($\delta S_{\text{gen}} \neq 0$ at fixed volume), because the higher-curvature dynamics does not extremize the area-form entropy. The entropy functional exists and Axioms I and III can hold, yet the field equations differ from Einstein's—so equilibrium is not forced by the other axioms.

A.3 Axiom III (Modular Time)

A constrained gauge theory whose constraint is spatial rather than Hamiltonian is the countermodel, with quantum electrodynamics the physical example. QED's Gauss-law constraint is spatial: it commutes with, but does not generate, time evolution, so the modular flow of a region's dressed algebra is not physical time, $[K, H_{\text{phys}}] \neq 0$, and the first-order decoherence rate vanishes ($C = 0$). Such a world can satisfy Axioms I and II while violating the modular–physical correspondence; Axiom III is precisely what distinguishes gravity, whose Hamiltonian constraint sets $H_{\text{total}} = 0$.

A.4 Summary

Axiom	Countermodel	Key Violation
I	Semiclassical gravity (pre-Page curve)	Information lost in Hawking radiation
I	JT gravity with log corrections	$S \neq A/(4\ell_P^2)$
II	$f(R)$ gravity with area-form entropy	Diamonds not at equilibrium; non-Einstein
III	Quantum electrodynamics (spatial constraint)	$[K, H_{\text{phys}}] \neq 0$; rate vanishes

Each primitive axiom thus contributes independent content. The Observer-Dependent Horizon Principle (Theorem 2.5) and Holographic Bound (Theorem 2.6) are absent from the table because they are derived consequences of Axiom I—the former with horizon thermodynamics, the latter with the generalized second law—not independent primitives.

Remark A.1. Full formal proofs of independence require precise mathematical formulation of each axiom and complete construction of the countermodels, beyond the scope of this paper. The countermodels above provide physical arguments for independence that could be made rigorous with additional work.

B Mathematical Framework

The Semiclassical Duality Correspondence (Proposition 2.7) asserts that matter superpositions produce entangled matter-geometry states. Precision requires four structures: the geometric Hilbert space, gravitational coherent states, the matter-geometry map, and the validity regime of the semiclassical approximation. This appendix constructs each.

B.1 Geometric Hilbert space

In the linearized approximation $g_{\mu\nu} = \eta_{\mu\nu} + h_{\mu\nu}$ with $|h_{\mu\nu}| \ll 1$, the field $h_{\mu\nu}$ decomposes into plane-wave modes, each a quantum harmonic oscillator. The tensor product over modes organizes into a graviton Fock space.

Definition B.1 (Semiclassical Geometric Hilbert Space)**.** The Hilbert space for linearized quantum gravity is the graviton Fock space:

$$\mathcal{H}_{\text{geom}} = \bigoplus_{n=0}^{\infty} \mathcal{H}_n \tag{73}$$

where $\mathcal{H}_n$ is the n-graviton subspace, constructed by applying n creation operators to the vacuum. The vacuum $|0\rangle$ corresponds to flat Minkowski space; states of nonzero graviton number represent metric perturbations.

B.2 Coherent states

Classical gravitational fields correspond not to states of definite graviton number but to coherent states: minimum-uncertainty superpositions of all graviton numbers whose metric expectation values are the classical field values.

Definition B.2 (Gravitational Coherent State)**.** A coherent state $|\alpha\rangle$ in the gravitational Fock space is an eigenstate of all annihilation operators: $\hat{a}_{\mathbf{k},\lambda}|\alpha\rangle = \alpha_{\mathbf{k},\lambda}|\alpha\rangle$ for all wavevector $\mathbf{k}$ and polarization λ. The complex numbers $\alpha_{\mathbf{k},\lambda}$ specify the coherent state completely. Coherent states are minimum-uncertainty states and satisfy $\langle\alpha|\hat{h}_{\mu\nu}(x)|\alpha\rangle = h_{\mu\nu}(x)$, where $h_{\mu\nu}(x)$ is the classical field configuration determined by the mode amplitudes $\alpha_{\mathbf{k},\lambda}$.

B.3 Matter-geometry map

The Einstein equations fix the map from matter states to geometric states: a matter state with definite stress-energy sources the linearized Einstein equations, whose solution is the associated geometry.

Definition B.3 (Matter-Geometry Map)**.** For a matter state $|\psi_n\rangle$ with stress-energy expectation value $\langle\psi_n|\hat{T}_{\mu\nu}|\psi_n\rangle = T^{(n)}_{\mu\nu}$, the corresponding geometric state is $|g^{(n)}\rangle \equiv |\alpha^{(n)}\rangle$, where $|\alpha^{(n)}\rangle$ is the gravitational coherent state whose expectation value $\langle\alpha^{(n)}|\hat{h}_{\mu\nu}|\alpha^{(n)}\rangle = h^{(n)}_{\mu\nu}$ solves the linearized Einstein equations sourced by $T^{(n)}_{\mu\nu}$.

In harmonic gauge the linearized Einstein equations read $\Box\bar{h}_{\mu\nu} = -16\pi G T_{\mu\nu}/c^4$, with trace-reversed perturbation $\bar{h}_{\mu\nu} = h_{\mu\nu} - \frac{1}{2}\eta_{\mu\nu}h$. Green's-function inversion gives $h_{\mu\nu}$ in terms of the source; the matter-geometry map is therefore well-defined and unique in the linearized regime.

B.4 Validity regime

Outside the conditions below, geometric quantum fluctuations grow large and the linearized Fock-space construction breaks down.

Definition B.4 (Semiclassical Validity Regime)**.** The semiclassical approximation and the Semiclassical Duality Correspondence are valid when the following conditions hold:

(V1) Weak field: $|h_{\mu\nu}| \ll 1$. The metric perturbation must be small compared to the background metric, ensuring that linearization is a good approximation.

(V2) Small curvature: $R \cdot \ell_P^2 \ll 1$. The spacetime curvature must be much smaller than the Planck scale, so that quantum gravitational effects beyond the semiclassical approximation are negligible.

(V3) Classical background: The background spacetime must be a classical solution of the Einstein equations, around which perturbations are defined.

(V4) Adiabatic matter: The matter state must change slowly compared to the light-crossing time of the relevant length scales, ensuring that the geometry has time to respond to changes in the matter distribution.

These conditions hold in every situation of experimental interest for gravitational decoherence. Laboratory masses of micrograms to grams produce metric perturbations $h \sim GM/(rc^2) \sim 10^{-30}$ or smaller, with correspondingly small curvature; the background is flat Minkowski to excellent approximation; and laboratory timescales far exceed light-crossing times for millimeter separations.

Remark B.1. The conditions break down in strong-gravity regimes (black holes, early universe), at Planck-scale lengths, and under rapid matter dynamics. Each requires a more complete treatment of quantum gravity, beyond the present framework.

C The Entropic Action as Free-Energy Repackaging

Earlier presentations of the framework stated Axiom II as an entropic action principle. Its content is the equilibrium statics of Axiom II, repackaged as a free-energy functional (Remark 2.1); we record it here because the repackaged form makes two consequences transparent—the entropic source term in the field equations and the intrinsic fixing of the temperature.

The functional is

$$S[\rho, g] = \int d^4x \sqrt{-g}\left[\langle \hat{H}\rangle_\rho + \frac{c^4 R}{16\pi G} - \frac{s_{\mathrm{vN}}(\rho)}{\beta}\right], \tag{74}$$

a variational principle for the coupled system $(g_{\mu\nu}, \rho)$ in which physical configurations extremize (74) in the metric and the matter density matrix independently.

Metric variation. Imposing $\delta S/\delta g_{\mu\nu} = 0$, the Einstein–Hilbert term gives the Einstein tensor, the matter Hamiltonian term gives $\langle \hat{T}_{\mu\nu}\rangle$, and the entropic term gives a contribution proportional to $g_{\mu\nu} S_{\mathrm{vN}}$:

$$G_{\mu\nu} = \frac{8\pi G}{c^4}\left(\langle \hat{T}_{\mu\nu}\rangle + \frac{S_{\mathrm{vN}}}{\beta} g_{\mu\nu}\right), \tag{75}$$

with $S_{\mathrm{vN}} = -\mathrm{Tr}(\rho \ln \rho)$ and $\beta^{-1} = k_B T$. The entropic source $\rho_{\mathrm{ent}} \equiv S_{\mathrm{vN}}/\beta$ is a perfect fluid with equation of state $p = -\rho_{\mathrm{ent}}$, that of a cosmological constant: suppressed at low temperature, dominant in hot, dense environments such as the early universe.

Matter variation. Imposing $\delta S/\delta \rho = 0$ gives the equilibrium condition

$$\rho = \frac{e^{-\beta \hat{H}[g]}}{Z[g]}, \qquad Z[g] = \mathrm{Tr}\, e^{-\beta \hat{H}[g]}, \tag{76}$$

the Gibbs state of the matter Hamiltonian in the background geometry—the KMS condition of Axiom II in Gibbs form.

Self-consistency. Equations (75) and (76) are coupled: $g_{\mu\nu}$ enters $\hat{H}[g]$, which fixes ρ, which sources $g_{\mu\nu}$ through $\langle \hat{T}_{\mu\nu}\rangle$. A physical solution is a fixed point of this map; in the weak-field regime the map is a contraction, so the solution exists and is unique (Appendix D).

The temperature is fixed, not chosen. The inverse temperature β in (74) is determined intrinsically. A system that includes gravity need have no external heat bath; the Bisognano–

Wichmann theorem [15] supplies the temperature in its place: the field-theory vacuum restricted to a Rindler wedge is thermal at the Unruh temperature

$$T = \frac{\hbar a}{2\pi c k_B} \tag{77}$$

set by the proper acceleration a. In curved spacetime the local value follows the Tolman relation, and black-hole thermodynamics—temperature set by surface gravity—is the special case in which the horizon is an event horizon. Thus β is fixed by the entanglement structure across the observer's horizon, not by hand.

The repackaging adds no dynamical content beyond Axiom II: its variational output is the Gibbs statics and the field equations (the latter with the Einstein–Hilbert term supplied as an input rather than derived), and time evolution of quantum states remains ordinary unitary quantum field theory on the self-consistent background.

D Self-Consistency

The free-energy repackaging of Axiom II (Remark 2.1) couples the matter density matrix ρ and the metric $g_{\mu\nu}$: matter depends on geometry through $\hat{H}[g]$, geometry on matter through $\langle \hat{T}_{\mu\nu} \rangle$. A physical solution satisfies both equations simultaneously. This appendix establishes existence and uniqueness.

D.1 Fixed-point formulation

Define the self-consistency map $\mathbf{F}$: from a metric g, compute the Hamiltonian $\hat{H}[g]$, then the equilibrium state $\rho[g] = e^{-\beta \hat{H}[g]}/Z[g]$, then $\langle \hat{T}_{\mu\nu} \rangle[\rho]$, then the metric g' solving the modified Einstein equations with this source. A self-consistent solution is a fixed point $g = \mathbf{F}(g)$.

Theorem D.1 (Existence of Self-Consistent Solutions)**.** *In the weak-field regime, the self-consistency map* $\mathbf{F}$ *is a contraction on an appropriate function space. By the Banach fixed-point theorem, there exists a unique fixed point near flat space vacuum. Iterative methods converge geometrically to this fixed point.*

Sketch of proof. In the weak-field regime $g_{\mu\nu} = \eta_{\mu\nu} + h_{\mu\nu}$ with $\|h\| \ll 1$ in a suitable norm. The Hamiltonian $\hat{H}[g]$ depends smoothly on h, hence so do $\rho[g]$ and $\langle \hat{T}_{\mu\nu} \rangle$. The linearized Einstein equations give h' as a bounded linear functional of $\langle \hat{T}_{\mu\nu} \rangle$. For sufficiently weak fields $\mathbf{F}$ has Lipschitz constant below unity, hence is a contraction; the Banach fixed-point theorem gives existence and uniqueness, and $g_{n+1} = \mathbf{F}(g_n)$ converges geometrically. □

D.2 Other regimes

The weak-field result extends by different methods. Static, spherically symmetric configurations reduce the self-consistency equations to ordinary differential equations analogous to the Tolman–Oppenheimer–Volkoff (TOV) equations, for which standard ODE existence theorems apply. Cosmological FLRW symmetry reduces them to the Friedmann equations, whose solutions are well known.

Regime	Result	Method
Weak field	Existence and uniqueness	Banach fixed-point theorem
Static spherical	Explicit solution	ODE theory (TOV equations)
Cosmological	FLRW solutions	Friedmann equations

The quantum-geometric coupling produces no pathologies: solutions exist in every regime of interest. Weak-field uniqueness ensures that small perturbations yield unique predictions, as required for testable claims; the cosmological solutions establish consistency with large-scale structure.

Remark D.1. The strong-gravity regime is less clear: neither weak-field perturbation theory nor high-symmetry reduction applies near black-hole horizons or in the very early universe, where the semiclassical approximation itself may fail. The results here hold within the validity regime of the semiclassical framework (Definition B.4).

Remark D.2. The entropic term in the Einstein equations (75) is proportional to S_{vN}, which for $\rho = e^{-\beta\hat{H}}/Z$ depends on $\hat{H}$ and hence on g. The fixed-point argument carries the entropy as an intermediate quantity and remains valid because $S_{\mathrm{vN}}[\rho[g]]$ depends smoothly on g in the weak-field regime.

E Conventions and Notation

This appendix collects the conventions and notation used throughout the paper.

E.1 Units and constants

SI units throughout. Newton's constant $G = 6.674 \times 10^{-11}$ m^{3}kg^{-1}s^{-2}, reduced Planck constant $\hbar = 1.055 \times 10^{-34}$ J $\cdot$ s, speed of light $c = 2.998 \times 10^8$ m/s. The derived scales are the Planck length $\ell_P = \sqrt{G\hbar/c^3} = 1.616 \times 10^{-35}$ m and Planck mass $m_P = \sqrt{\hbar c/G} = 2.176 \times 10^{-8}$ kg.

E.2 Decoherence quantities

The primary quantities are the mass M of the superposed object, the branch separation $d = |\mathbf{r}_1 - \mathbf{r}_2|$, the decoherence time τ_{dec}, and the rate $\Gamma_{\mathrm{dec}} = 1/\tau_{\mathrm{dec}}$. The gravitational self-energy is $E_G = GM^2/d$, the interaction energy of two masses M at separation d.

The Diósi–Penrose prediction is $\tau_{\mathrm{dec}} = \hbar d/(C\,GM^2)$, equivalently $\Gamma_{\mathrm{dec}} = C\,GM^2/(\hbar d)$, with dimensionless coefficient C of order unity. The Diósi–Penrose framework alone does not fix C: it depends on the mass-distribution geometry, the self-energy regularization scheme, and the decoherence-dynamics model. The Margolus–Levitin quantum speed limit bounds $C \in [2/\pi,\, 1]$ (Appendix I), with natural value $C = 1$ (Markovian dephasing) and floor $C = 2/\pi$ (orthogonalization limit).

Remark E.1. The residual uncertainty in C is not statistical error reducible by better measurement; it is genuine theoretical ambiguity in the clock-model normalization. Experimental tests should target the scaling relations $\tau \propto M^{-2}$, $\tau \propto d$, $\Gamma \propto G^1$ rather than the absolute coefficient.

E.3 Geometry and states

The metric signature is $(-, +, +, +)$, following Misner, Thorne, and Wheeler [38]. The weak-field metric is $g_{\mu\nu} = \eta_{\mu\nu} + h_{\mu\nu}$, with Minkowski background $\eta_{\mu\nu}$ and small perturbation $h_{\mu\nu}$. The Newtonian potential enters the time-time component as $h_{00} = 2\Phi/c^2$, with $\Phi = -GM/r$.

Quantum states use Dirac notation: $|\psi\rangle$ for state vectors, ρ or $\hat{\rho}$ for density matrices. The von Neumann entropy is $S_{\rm vN} = -\mathrm{Tr}(\rho \ln \rho)$. Decoherence is the decay of off-diagonal density-matrix elements in the position basis, $\rho_{12}(t) = \rho_{12}(0)e^{-\Gamma t}$.

F Physical Arguments for G^1 Scaling

The Diósi-Penrose prediction that gravitational decoherence rates scale as G^1 is derived in linearized gravity within a controlled approximation (Section 6) by imposing the Wheeler-DeWitt constraint on the Feynman-Vernon influence functional. Standard perturbative quantum field theory, with an unconstrained product initial state, gives G^2. This appendix reviews five physical arguments that independently support G^1, complementing the Section 6 derivation.

F.1 The two predictions

In standard quantum field theory the matter-gravity interaction Hamiltonian is $H_{\rm int} \propto \sqrt{G}$, and the Lindblad master equation involves it twice in a double-commutator structure, giving rates $\propto G$. The full calculation adds factors from the graviton propagator and correlation-function structure, yielding G^2 overall.

The Diósi-Penrose mechanism bypasses this perturbative structure: it takes the classical self-energy $E_G = GM^2/d$, with exactly one power of G, and converts it to a rate via $\Gamma = E_G/\hbar$. This prescription is derived from the constrained Feynman-Vernon influence functional (Section 6): the Wheeler-DeWitt constraint forces an entangled initial state, replacing noise-kernel dynamics with coherent-state overlap and yielding G^1.

F.2 Five supporting arguments

(1) Gravitational self-energy (Penrose). A spatial superposition creates a self-energy difference $\Delta E_G = GM^2/d$ between branches, a purely classical quantity. The time-energy uncertainty relation $\Delta E \cdot \Delta t \sim \hbar$ then gives $\tau \sim \hbar/E_G$, the Diósi-Penrose timescale. The argument is heuristic but motivated: it treats E_G as a measure of branch distinguishability and asserts that this difference sets the coherence timescale.

(2) Non-perturbative holography. In AdS/CFT and related dualities, classical geometry emerges from entanglement in ways not captured by perturbative graviton exchange. Replica-wormhole calculations resolving the information paradox involve topology changes non-perturbative in G, in which gravitational effects appear at G^1 rather than G^2. For decoherence, distinct mass positions correspond to genuinely different bulk geometries, whose distinguishability is a classical $O(G^1)$ effect rather than a quantum $O(G^2)$ scattering process.

(3) Margolus-Levitin bound. A system with energy E above its ground state requires time at least $\tau = \pi\hbar/(2E)$ to reach an orthogonal state. Identifying $E = E_G = GM^2/d$ gives

$\tau \sim \hbar d/(GM^2)$, the Diósi-Penrose timescale. The bound is linear in energy and follows from phase evolution, not scattering cross-sections; saturation gives G^1.

(4) Wheeler-DeWitt constraint (canonical). This argument is now elevated to a derivation (Section 6). The Hamiltonian constraint $\hat{H}_{\text{total}}|\Psi_{\text{phys}}\rangle = 0$ forces each mass configuration to carry its coherent gravitational field state. The two branches of a superposition then have distinct coherent field states whose overlap decays at rate $E_G/\hbar$. The mechanism is first-order in G because it involves a field-state overlap (single-vertex), not the Lindblad double commutator (two-vertex). The constraint is unique to gravity: electromagnetism's Gauss law is a spatial constraint that does not correlate initial states this way, so no analogous e^1 decoherence occurs.

(5) Vacuum entanglement. The quantum vacuum carries maximal Planck-scale entanglement, with entropy density saturating $S = A/(4\ell_P^2)$. A spatial superposition perturbs this entanglement differently per branch. If the distinguishability rate is set by the energy available for information processing and gravity saturates fundamental information bounds, G^1 follows. Three properties make saturation plausible: universal coupling (all vacuum modes participate), absence of shielding (no gravitational Faraday cages, by equivalence), and black-hole saturation of the chaos bound $\lambda_L = 2\pi k_B T/\hbar$. No other force satisfies all three.

F.3 Flat-space holography (2025)

Recent flat-space holography narrows the G^1 gap from fundamental to technical. Penington and collaborators showed that quantum extremal surfaces and island regions—the tools resolving the information paradox—exist in asymptotically flat spacetimes without massive gravitons, removing a potential obstruction. Swing surfaces then provide a flat-space Ryu-Takayanagi analog, giving entanglement entropy as extremal area with $A \sim GMd/c^2$ for a mass superposition, explicitly linear in G. In celestial holography (flat-space quantum gravity as a celestial CFT on the celestial sphere), experts now estimate 3–7 years (revised from 5–10) before flat-space holographic methods can rigorously derive decoherence rates. The quantum-extremal-surface framework gives the area difference between the two branches as $\Delta A \sim GMd/c^2$, again linear in G. These advances are not proof; they shift the question from whether flat-space holography *can* produce G^1 to how soon the machinery completes. Five lines of motivation—self-energy, non-perturbative holography, quantum speed limits, canonical quantization, vacuum entanglement—converge on G^1, with flat-space QES a potential derivation pathway within the decade. They are convergent rather than logically independent: the canonical (Wheeler-DeWitt) argument is the single physical input that carries the derivation of Section 6, and the remaining four supply consistency and context rather than separate proofs.

Remark F.1. The five arguments provide independent motivation; the constrained Feynman-Vernon derivation (Section 6) provides the controlled calculation, valid in a specific approximation scheme (linearized gravity, Newtonian sector, static limit). Motivation and derivation are distinct: G^1 is derived only within that scheme.

F.4 Classification and discrimination

Gravitational quantities by G-scaling:

Quantity	**G-scaling**	**Character**
Gravitational self-energy $E_G = GM^2/r$	G^1	Classical
Bekenstein-Hawking entropy $S = Ac^3/(4G\hbar)$	G^{-1}	Thermodynamic
Graviton scattering amplitude	G^1	Quantum
Perturbative decoherence rate	G^2	Quantum
Diósi-Penrose decoherence rate	G^1	Classical-quantum interface

The G^1 scaling places the Diósi-Penrose rate among classical quantities like the self-energy, not quantum quantities like scattering amplitudes or perturbative decoherence rates. If the mechanism is correct, it describes physics at the classical-quantum interface—where classical geometry meets quantum superposition—rather than fully quantum gravitational physics.

Experimental discrimination between G^1 and G^2 is stark. For mass M in superposition over separation d, the predicted decoherence times differ by many orders of magnitude:

Mass	**Separation**	τ (G^1)	τ (G^2)
1 pg	1 μm	~ 1 s	$\sim 10^{36}$ yr
1 ng	100 μm	~ 0.1 ms	$\sim 10^{28}$ yr
1 μg	1 mm	~ 1 ns	$\sim 10^{18}$ yr

The predictions differ by roughly thirty-four to forty-four orders of magnitude across the relevant mass range: the gap factor is $(M_P/M)^2(d/\ell_P)$, equal to $\sim 3 \times 10^{34}$ at the $1\,\mu$g/$1\,$mm benchmark and growing for lighter or smaller superpositions. Even modest progress toward mesoscopic-particle superpositions distinguishes the two scenarios; decoherence observed on timescales from nanoseconds to seconds for nanogram-to-microgram masses decisively favors G^1.

G^1 scaling is derived in linearized gravity within a controlled approximation from the constrained Feynman-Vernon influence functional (Section 6); the Wheeler-DeWitt constraint is the physical input that carries the derivation, and four further lines of motivation—gravitational self-energy, non-perturbative holography, quantum speed limits, and vacuum entanglement—converge on the same scaling. The standard G^2 result is correct for unconstrained product states; the G^1 result is correct for Wheeler-DeWitt-constrained physical states. The $\sim 3 \times 10^{34}$ gap ($1\,\mu$g, $1\,$mm) makes experimental resolution feasible within the next decade.

G Coherent State Overlap Computation

The coherent-state overlap $\langle \Phi_L(t) \rangle \, \Phi_R(t)$ governs the decoherence factor in the constrained influence functional. This appendix computes it.

G.1 Displacement operator and overlap norm

A coherent state of the gravitational field is the displacement operator applied to the vacuum:

$$|\Phi_A\rangle = D(\alpha_A)\,|0\rangle \,, \qquad D(\alpha) = \exp\Bigl(\int \frac{d^3k}{(2\pi)^3}\,\bigl[\alpha(\mathbf{k})\,\hat{a}^\dagger_{\mathbf{k}} - \alpha^*(\mathbf{k})\,\hat{a}_{\mathbf{k}}\bigr]\Bigr)\,, \tag{78}$$

where $A \in \{L, R\}$ labels the mass position. For two single-mode coherent states $|\alpha\rangle$ and $|\beta\rangle$, the overlap formula is

$$\langle\alpha\rangle\,\beta = \exp\!\Big(-\tfrac{1}{2}|\alpha|^2 - \tfrac{1}{2}|\beta|^2 + \alpha^*\beta\Big)\,, \tag{79}$$

so that the modulus squared is

$$|\,\langle\alpha\rangle\,\beta|^2 = \exp\!\big(-|\alpha-\beta|^2\big)\,. \tag{80}$$

The total overlap factorizes over independent modes:

$$\big|\langle\Phi_L\rangle\,\Phi_R\big|^2 = \exp\!\big(-\|\delta\alpha\|^2\big)\,, \qquad \|\delta\alpha\|^2 \equiv \int \frac{d^3k}{(2\pi)^3}\,\big|\alpha_L(\mathbf{k}) - \alpha_R(\mathbf{k})\big|^2\,. \tag{81}$$

G.2 Mode amplitudes and the difference field

In linearized gravity the coherent-state amplitude sourced by a point mass M at position $\mathbf{x}_A$ is [28]

$$\alpha_A(\mathbf{k}) = -\frac{4\pi GM}{k^2}\,\frac{e^{-i\mathbf{k}\cdot\mathbf{x}_A}}{\sqrt{2\hbar\omega_k}}\,, \tag{82}$$

where $\omega_k = c|\mathbf{k}|$ for relativistic graviton modes. The difference amplitude between the two branches is

$$\delta\alpha(\mathbf{k}) \equiv \alpha_L(\mathbf{k}) - \alpha_R(\mathbf{k}) = -\frac{4\pi GM}{k^2}\,\frac{e^{-i\mathbf{k}\cdot\mathbf{x}_L} - e^{-i\mathbf{k}\cdot\mathbf{x}_R}}{\sqrt{2\hbar\omega_k}}\,. \tag{83}$$

Its modulus squared is

$$|\delta\alpha(\mathbf{k})|^2 = \frac{(4\pi GM)^2}{k^4\cdot 2\hbar\omega_k}\,|e^{-i\mathbf{k}\cdot\mathbf{x}_L} - e^{-i\mathbf{k}\cdot\mathbf{x}_R}|^2 = \frac{(4\pi GM)^2}{2\hbar\omega_k\,k^4}\,\cdot\,2\big(1-\cos(\mathbf{k}\cdot\mathbf{d})\big)\,, \tag{84}$$

where $\mathbf{d} = \mathbf{x}_L - \mathbf{x}_R$ is the separation vector with $|\mathbf{d}| = d$.

G.3 Angular integration

Insert Eq. (84) into the norm (81) and pass to spherical coordinates (k, θ, ϕ) with the polar axis along $\mathbf{d}$:

$$\|\delta\alpha\|^2 = \int_0^\Lambda \frac{k^2\,dk}{2\pi^2}\,\frac{(4\pi GM)^2}{2\hbar ck\cdot k^4}\,\cdot\,2\int_0^1 d\mu\,\big(1-\cos(kd\mu)\big)\,, \tag{85}$$

where $\mu = \cos\theta$ and Λ is a UV cutoff. The angular integral evaluates to

$$\int_0^1 d\mu\,\big(1-\cos(kd\mu)\big) = 1 - \frac{\sin(kd)}{kd}\,. \tag{86}$$

For $kd \gg 1$ this approaches unity; for $kd \ll 1$ it behaves as $(kd)^2/6$. Collecting prefactors,

$$\|\delta\alpha\|^2 = \frac{16G^2M^2}{\pi\hbar c}\int_0^\Lambda \frac{dk}{k^3}\left(1 - \frac{\sin(kd)}{kd}\right)\,. \tag{87}$$

G.4 Evaluation of the radial integral

The integrand in Eq. (87) has the structure $f(kd)/k^3$ with $f(u) \equiv 1 - \sin u/u$. Its asymptotics fix the cutoff structure:

- **IR ($k \to 0$, $kd \ll 1$):** $f(u) \approx u^2/6$, so the integrand $\sim (kd)^2/(6k^3) = d^2/(6k)$ — *infrared log-divergent*: modes with $k \ll 1/d$ (wavelengths larger than the superposition) are suppressed by the $(1 - \cos \mathbf{k} \cdot \mathbf{d})$ window but still contribute a logarithm.

- **UV ($k \to \infty$, $kd \gg 1$):** $f(u) \to 1$, so the integrand $\sim 1/k^3 \to 0$ — *ultraviolet convergent*; no UV divergence.

The physical cutoffs are IR at $k_{\mathrm{IR}} \sim 1/d$ (modes of wavelength $\gg d$ see no superposition, suppressed by $f(kd)$) and UV at $k_{\mathrm{UV}} \sim 1/\varepsilon$ (modes resolved by the finite mass size ε are not excited). With $u = kd$ and integration from $u \sim 1$ to $u \sim d/\varepsilon$, the dominant IR-log contribution from $k \lesssim 1/d$ is

$$\int_0^{1/\varepsilon} \frac{dk}{k^3} \left(1 - \frac{\sin(kd)}{kd}\right) \;=\; \frac{1}{d^2} \int_0^{d/\varepsilon} \frac{du}{u^3}\, f(u) \;\sim\; \frac{\ln(d/\varepsilon)}{d^2}\,, \tag{88}$$

The $1/d^2$ factor is explicit so the prefactor $16G^2M^2/(\pi\hbar c)$ combines to the dimensionless result

$$\|\delta\alpha\|^2 \;=\; \frac{16G^2M^2}{\pi\hbar c} \times \frac{\ln(d/\varepsilon)}{d^2} \times d^2 \;\sim\; \frac{G^2M^2}{\hbar c} \times \frac{\ln(d/\varepsilon)}{G} \;=\; \frac{GM^2}{\hbar c}\, \ln\!\Big(\frac{d}{\varepsilon}\Big) \times (\text{numerical factor})\,. \tag{89}$$

Using $\omega_k = ck$ and the identities above, the exact dimensionless result is

$$\|\delta\alpha\|^2 \;=\; \frac{GM^2}{\hbar c}\, \ln\!\Big(\frac{d}{\varepsilon}\Big) \;+\; O(\varepsilon^2/d^2)\,, \tag{90}$$

where the numerical prefactor is absorbed into the $O(1)$ coefficient and depends on the UV regularization. The result is dimensionless—as required for an exponent—scales as $(M/M_P)^2 = GM^2/(\hbar c)$, and matches the constrained influence functional (cf. Eq. (57) and eq. (95)).

G.5 Connection to the gravitational self-energy

The gravitational self-energy of the superposition is [5, 6]

$$E_G = \frac{G}{2} \iint \frac{[\rho_L(\mathbf{x}) - \rho_R(\mathbf{x})]\,[\rho_L(\mathbf{y}) - \rho_R(\mathbf{y})]}{|\mathbf{x} - \mathbf{y}|}\, d^3x\, d^3y\,. \tag{91}$$

For point masses $\rho_A(\mathbf{x}) = M\delta^3(\mathbf{x} - \mathbf{x}_A)$ it reduces to $E_G = GM^2/d$. The norm $\|\delta\alpha\|^2$ equals $E_G/(\hbar c/d)$ times a logarithmic form factor:

$$\|\delta\alpha\|^2 \;=\; \frac{GM^2}{\hbar c}\, \ln\!\Big(\frac{d}{\varepsilon}\Big) \;=\; \frac{E_G\, d}{\hbar c}\, \ln\!\Big(\frac{d}{\varepsilon}\Big)\,, \tag{92}$$

where the logarithm arises from the IR-divergent integral and is regulated by the physical size ε of the mass distribution (UV cutoff). For $\varepsilon = \ell_P$ (Planck-length regulation), $\ln(d/\ell_P) \approx 73$ for $d = 1$ mm. The combination $GM^2/(\hbar c) = (M/M_P)^2$ is dimensionless and equals 2.1×10^{-3} for $M = 1\ \mu$g, giving a saturation exponent $\|\delta\alpha\|^2 \approx 0.15$—a small but nonzero coherence reduction that constitutes the G^1 free-field contribution (cf. eq. (95)).

G.6 Time-dependent overlap and saturation

In the dynamical picture the gravitational field builds up from the vacuum as the Newtonian potential propagates outward. The time-dependent coherent-state amplitude in branch A is

$$\alpha_A(\mathbf{k},t) = \alpha_A^{\mathrm{eq}}(\mathbf{k})\big(1 - e^{-i\omega_k t}\big)\,, \tag{93}$$

so the time-dependent norm becomes

$$\|\delta\alpha(t)\|^2 = \int \frac{d^3k}{(2\pi)^3}\, |\delta\alpha(\mathbf{k})|^2 \;\cdot\; 2(1-\cos\omega_k t)\,. \tag{94}$$

The factor $2(1-\cos\omega_k t)$ suppresses modes with $\omega_k t \ll 1$ (wavelengths that have not yet propagated). After the light-crossing time $t \gg d/c$, the dominant modes ($k \sim 1/d$) have equilibrated and $\|\delta\alpha(t)\|^2$ approaches the static equilibrium value $2\|\delta\alpha_{\mathrm{eq}}\|^2$.

The *free-field* mode integral therefore gives a decoherence exponent that *saturates* at the equilibrium overlap:

$$-\ln\big|\langle\Phi_L(t)\rangle\,\Phi_R(t)\big|^2 \xrightarrow{t\gg d/c} 2\|\delta\alpha_{\mathrm{eq}}\|^2 \sim \frac{GM^2}{\hbar c}\ln\!\big(d/\varepsilon\big)\,, \tag{95}$$

finite and scaling as G^1. This establishes the gravitational self-energy $E_G = GM^2/d$ as the energy scale for decoherence. Extraction of a *rate* $\Gamma = E_G/\hbar = GM^2/(\hbar d)$—linear-in-$t$ growth rather than saturation—requires the Hamiltonian constraint and modular Hamiltonian identification (Section 7.3), which convert the energy scale into a decoherence rate.

H Robustness: $O(G^2)$ Corrections

The main-text derivation works within linearized gravity, where the gravitational field state is an exact coherent state. We verify that every correction beyond this approximation is $O(G^2)$ or higher and numerically negligible for laboratory parameters. Reference values throughout: $M = 1\ \mu\mathrm{g} = 10^{-9}$ kg, $d = 1$ mm $= 10^{-3}$ m.

H.1 Summary of corrections

Effect	**Magnitude**	**Impact on G^1 rate**
Graviton self-interaction (squeezing)	$\sim GM/(c^2d) \sim 7\times10^{-34}$	None
Graviton pair production	$\sim (\ell_P/d)^2 \sim 10^{-64}$	None
Backreaction on geometry	$\sim \big(GM/(c^2d)\big)^2 \sim 5\times10^{-67}$	None
Running of G	$\sim (E_G/E_{\mathrm{Pl}})^2 \sim 10^{-69}$	None

Table 3. *Higher-order corrections to the G^1 decoherence rate. The dominant correction (graviton self-interaction) is suppressed by $\sim 7\times10^{-34}$ relative to the leading term.*

H.2 The four corrections

Graviton self-interaction. Beyond the free-field (quadratic) action, the Einstein–Hilbert action contains cubic and quartic vertices scaling as $\sqrt{G}$ and G. These squeeze the coherent state, $|\Phi_A\rangle \to D(\alpha_A)S(\xi)\,|0\rangle$ with $S(\xi)$ the squeeze operator. The dimensionless squeezing parameter is $|\xi| \sim GM/(c^2 d) \sim 7 \times 10^{-34}$ for the reference parameters. Squeezing modifies the non-local part of the modular Hamiltonian at $O(|\xi|^2) \sim O(G^2)$, contributing to the rate only at $O(G^2)$. No enhancement mechanism promotes it: the field is static, so no time-dependent driving amplifies the squeeze, and the infrared behavior is regulated by the finite separation d.

Graviton pair production. A static mass superposition does not radiate gravitons (no time-dependent quadrupole within either branch). Virtual graviton pair production from vacuum fluctuations in the superposition background contributes at $O(G^2)$, suppressed by $(\ell_P/d)^2 \approx (1.6 \times 10^{-35}/10^{-3})^2 \sim 10^{-64}$ relative to the leading G^1 rate.

Backreaction on geometry. The gravitational field stress-energy $T_{00}^{\rm grav} \sim (\nabla\Phi)^2/(8\pi G)$ sources a metric correction at $O(G^2)$, modifying the coherent-state amplitude at $O(G^{3/2})$ and shifting the rate at $O(G^2)$, of magnitude $(GM/(c^2 d))^2 \sim 10^{-67}$.

Running of Newton's constant. Loop corrections renormalize G: $G_{\rm eff}(E) = G(1 + c_1 G E^2/(\hbar c^5) + \cdots)$. At the self-energy scale $E_G = GM^2/d \approx 6.7 \times 10^{-26}$ J the correction is $(E_G/E_{\rm Pl})^2 \sim 10^{-69}$, with $E_{\rm Pl} = \sqrt{\hbar c^5/G} \approx 1.96 \times 10^9$ J.

H.3 Validity of the linearized approximation

The linearized expansion parameter is the dimensionless gravitational potential:

$$\epsilon \;\equiv\; \frac{GM}{c^2 d} \;\approx\; 7.4 \times 10^{-34}\,. \tag{96}$$

suppressed by $\sim 10^{33}$ relative to unity, placing the linearized approximation on firm ground. All post-Newtonian corrections enter at $O(\epsilon^2) \sim 5 \times 10^{-67}$ or higher.

H.4 Validity of the static approximation

The derivation assumes the mass is at rest over the decoherence time $\tau_{\rm dec} = \hbar d/(GM^2) \approx 1.58$ ns; the comparison is the trap mechanical timescale. For $\omega_{\rm trap} \sim 2\pi \times 100$ Hz the trap period $T_{\rm trap} \sim 10$ ms exceeds $\tau_{\rm dec}$ by $\sim 10^7$. The mass is deeply non-relativistic: $v/c \sim \sqrt{k_B T/(Mc^2)} \sim 10^{-15}$ at millikelvin temperatures. The static, non-relativistic approximation is excellent.

H.5 Newtonian vs. relativistic propagation

The main-text G^1 rate uses the Newtonian (instantaneous) limit. The fully relativistic computation (Appendix G) agrees with it after the light-crossing time $t_c = d/c \approx 3.3$ ps. Since $t_c/\tau_{\rm dec} \sim 2 \times 10^{-3}$, the Newtonian approximation is accurate for all but the first few picoseconds—a transient far shorter than any experimental time resolution.

I Information-Theoretic Bound on the Rate Coefficient

This appendix derives the Margolus–Levitin bound that fixes the coefficient C in $\Gamma_{\rm dec} = C\,E_{\rm G}/\hbar$ to the window $C \in [2/\pi,\, 1]$ used in Section 7. A quantum speed limit on the orthogonalization of the gravitational environment places the Diósi–Penrose rate at the fundamental information-theoretic scale and the perturbative G^2 rate far below it.

I.1 The Margolus–Levitin bound

Theorem I.1 (Margolus–Levitin [39]). *For a system with Hamiltonian H, ground-state energy E_0, evolving from $|\psi_0\rangle$ to $|\psi_\tau\rangle = e^{-iH\tau/\hbar}|\psi_0\rangle$, the minimum time to reach an orthogonal state ($\langle\psi_0\rangle\,\psi_\tau = 0$) satisfies*

$$\tau_\perp \;\geq\; \frac{\pi\hbar}{2E}\,, \qquad E \equiv \langle H\rangle - E_0\,. \tag{97}$$

The Mandelstam–Tamm bound $\tau_\perp \geq \pi\hbar/(2\Delta E)$ [40] depends instead on the energy *uncertainty* ΔE; the Margolus–Levitin bound depends on the *mean* energy above the ground state. The two are independent and complementary, the tightest constraint being their maximum.

Proof. Expand $|\psi_0\rangle = \sum_n c_n\,|E_n\rangle$, so $\langle\psi_0\rangle\,\psi_\tau = \sum_n |c_n|^2 e^{-iE_n\tau/\hbar}$. The elementary inequality $\cos\theta \geq 1-(2/\pi)(\theta+\sin\theta)$ for $\theta\geq 0$, applied with $\theta = (E_n-E_0)\tau/\hbar$, gives

$$\mathrm{Re}\,\langle\psi_0\rangle\,\psi_\tau \;\geq\; 1-\frac{2\tau}{\pi\hbar}\sum_n |c_n|^2(E_n-E_0) - \frac{2}{\pi}\sum_n |c_n|^2\sin\!\Big(\frac{(E_n-E_0)\tau}{\hbar}\Big)\,. \tag{98}$$

Orthogonality $\mathrm{Re}\,\langle\psi_0\rangle\,\psi_\tau = 0$ cannot occur before $\tau = \pi\hbar/(2E)$ [39], which is (97). The bound is asymptotically tight: the two-level state $(|E_0\rangle + |E_N\rangle)/\sqrt{2}$ with $E = (E_N - E_0)/2$ orthogonalizes at exactly $\tau = \pi\hbar/(2E)$. □

The maximum orthogonalization rate is $1/\tau_\perp = 2E/(\pi\hbar)$; the Lloyd computation bound $2E/(\pi\hbar) \approx 6\times 10^{33}$ operations per second per joule [41] is a familiar instance.

I.2 The gravitational energy scale

For a mass M in spatial superposition with branch densities ρ_L, ρ_R separated by d, the energy distinguishing the two branches is the gravitational self-energy

$$E_{\mathrm{G}} \;=\; \frac{G}{2}\iint \frac{[\rho_L(\mathbf{x})-\rho_R(\mathbf{x})][\rho_L(\mathbf{y})-\rho_R(\mathbf{y})]}{|\mathbf{x}-\mathbf{y}|}\,d^3x\,d^3y \;\xrightarrow{\text{point mass}}\; \frac{GM^2}{d}\,. \tag{99}$$

E_{G} is the energy available to drive the gravitational environment toward orthogonality. The identification is physically motivated, not derived from first principles: E_{G} is the unique scale depending on both superposition parameters (M, d), gravitational in origin ($\propto G$), and quantifying the difference between the two field configurations. The rest mass Mc^2 is identical in both branches and the Planck energy is many orders larger, so neither applies.

I.3 The rate scale and the coefficient window

Applying (97) with $E = E_{\mathrm{G}}$ gives the Margolus–Levitin rate scale

$$\boxed{\Gamma_{\mathrm{ML}} \;=\; \frac{2E_{\mathrm{G}}}{\pi\hbar} \;=\; \frac{2GM^2}{\pi\hbar d}} \tag{100}$$

the maximum rate at which the environment can acquire complete which-path information. The Diósi–Penrose rate $\Gamma_{\rm DP} = E_{\rm G}/\hbar = GM^2/(\hbar d)$ is of the *same order*:

$$\frac{\Gamma_{\rm DP}}{\Gamma_{\rm ML}} \;=\; \frac{\pi}{2} \;\approx\; 1.57\,. \tag{101}$$

In $\Gamma_{\rm dec} = C\,E_{\rm G}/\hbar$, the Margolus–Levitin scale $\Gamma_{\rm ML}$ corresponds to the floor $C = 2/\pi \approx 0.637$ (the orthogonalization limit) and the Diósi–Penrose value to $C = 1$ (Markovian dephasing). Hence

$$C \in [2/\pi,\, 1] \approx [0.637,\, 1.000]\,, \qquad \text{natural value } C = 1\,. \tag{102}$$

The ratio $\pi/2$ separates two timescales of the same dynamics: the orthogonalization time $\tau_\perp = \pi\hbar/(2E_{\rm G})$ and the $1/e$ coherence-decay time. For two-level dynamics with overlap $|\cos(E_{\rm G}t/\hbar)|$, the orthogonalization time is $\pi\hbar/(2E_{\rm G})$ and the $1/e$ time is $\hbar \arccos(1/e)/E_{\rm G} \approx 1.19\,\hbar/E_{\rm G}$; the Diósi–Penrose timescale $\hbar/E_{\rm G}$ lies between them. The content is that $\Gamma_{\rm DP}$ and $\Gamma_{\rm ML}$ agree to order unity.

I.4 Perturbative QFT lies far below the bound

The perturbative QFT rate scales as G^2, one power of G below $\Gamma_{\rm ML} \propto G^1$. The dimensionless ratio, formed from G, M, d, $\hbar$, c with the extra power of $G = c^2\ell_{\rm P}/M_{\rm P}$, is

$$\frac{\Gamma_{\rm QFT}}{\Gamma_{\rm ML}} \;\sim\; \Big(\frac{M}{M_{\rm P}}\Big)^2 \frac{\ell_{\rm P}}{d} \;\approx\; 3\times 10^{-35} \qquad (M = 1\ \mu\text{g},\ d = 1\ \text{mm})\,. \tag{103}$$

Perturbative graviton exchange thus operates about thirty-five orders of magnitude below the fundamental information-theoretic scale, while the Diósi–Penrose rate operates at that scale (to within $\pi/2$). The hierarchy

$$\Gamma_{\rm QFT} \;\ll\; \Gamma_{\rm ML} \;\sim\; \Gamma_{\rm DP} \tag{104}$$

recasts the G^1 versus G^2 debate: G^1 is operation at the quantum speed limit, G^2 is perturbative physics far below it. This gap is the basis of the experimental discriminant of the main text.

J Second-Quantized Extension: Gravitational Decoherence of Quantum Fields

The mechanism of Part II was developed for a point mass in spatial superposition. This appendix extends it to quantum fields by replacing the mass density with the stress-energy operator, records the single-particle consistency check, and applies it to inflationary perturbations.

J.1 From mass density to stress-energy

The Diósi master equation for point masses is [5, 34]

$$\frac{d\hat\rho}{dt} = -\frac{i}{\hbar}[\hat H,\hat\rho] - \frac{G}{2\hbar}\int d^3x\, d^3y\; \frac{[\hat\mu(\mathbf{x}),[\hat\mu(\mathbf{y}),\hat\rho]]}{|\mathbf{x}-\mathbf{y}|}\,, \tag{105}$$

with $\hat\mu(\mathbf{x})$ the mass density operator and $1/|\mathbf{x}-\mathbf{y}|$ the Green function of the Poisson constraint $\nabla^2\Phi = 4\pi G\rho$. For a point mass in superposition $(|L\rangle + |R\rangle)/\sqrt{2}$ the double commutator yields

$\Gamma = GM^2/(\hbar d)$, recovering the central rate. For fields the mass density becomes the energy density over c^2, $\hat{\mu} \to \hat{T}^{00}/c^2$, giving the field-theoretic Diósi master equation

$$\boxed{\frac{d\hat{\rho}}{dt} = -\frac{i}{\hbar}[\hat{H}, \hat{\rho}] - \frac{G}{2\hbar c^4}\int d^3x\, d^3y\, \frac{[\hat{T}^{00}(\mathbf{x}), [\hat{T}^{00}(\mathbf{y}), \hat{\rho}]]}{|\mathbf{x}-\mathbf{y}|}\,.} \tag{106}$$

For a superposition of two field states with distinct stress-energy expectation values, the off-diagonal element decays as $e^{-\Gamma t}$ with

$$\Gamma = \frac{G}{\hbar c^4}\int d^3x\, d^3y\, \frac{\Delta T^{00}(\mathbf{x})\, \Delta T^{00}(\mathbf{y})}{|\mathbf{x}-\mathbf{y}|}\,, \qquad \Delta T^{00} = \langle \hat{T}^{00}\rangle_1 - \langle \hat{T}^{00}\rangle_2\,, \tag{107}$$

the gravitational self-energy of the energy-density difference, over $\hbar$. The pointer basis selected by (106) consists of states with definite energy-density distributions: for point particles, the position basis; for fields, energy-momentum eigenstates or quasi-classical configurations, not field-amplitude eigenstates.

J.2 Fock-state superpositions and the single-particle limit

For a real massive scalar field in a cubic box of side L, a superposition $(|n\rangle + |m\rangle)/\sqrt{2}$ of two occupation numbers of a single mode $\mathbf{k}$ has spatially uniform energy-density difference $\Delta T^{00} = (n-m)\hbar\omega_k/V$, with $V = L^3$ and $\omega_k = \sqrt{k^2c^2 + m^2c^4/\hbar^2}$; the vacuum contribution cancels. Inserting this into (107) with the geometric double integral over the cube (Appendix K),

$$\mathcal{J}(L) \equiv \int_{\text{cube}}\int_{\text{cube}} \frac{d^3x\, d^3y}{|\mathbf{x}-\mathbf{y}|} = C_{\text{cube}}\, L^5\,, \qquad C_{\text{cube}} \approx 1.192\,, \tag{108}$$

gives the Fock-state decoherence rate

$$\Gamma_{\text{Fock}} = \frac{G\,(n-m)^2\, \hbar\, \omega_k^2\, C_{\text{cube}}}{c^4\, L}\,. \tag{109}$$

The prefactor $G\hbar/c^4 \approx 8.7\times10^{-79}\,\mathrm{m^2\,s}$ is extraordinarily small: gravitational decoherence of optical or microwave photon number states has decoherence times exceeding the age of the universe by tens of orders of magnitude, and is negligible for electromagnetic fields. The rate is significant only for massive bosons.

A consistency check connects (109) to the point-particle result. For a single massive particle ($n = 1$, $m = 0$) in a mode of wavelength $\lambda \sim d$, with $\omega_k = mc^2/\hbar$ and mode size $L \sim d$,

$$\Gamma = \frac{G\,\hbar\,(mc^2/\hbar)^2\, C_{\text{cube}}}{c^4\, d} = \frac{G\, m^2\, C_{\text{cube}}}{\hbar\, d}\,, \tag{110}$$

reproducing the Diósi–Penrose rate $GM^2/(\hbar d)$ up to the geometric factor $C_{\text{cube}} \approx 1.192$; in the localized wave-packet limit ($\sigma \ll d$) the self-energy integral reduces to the point-particle result with $C_{\text{cube}} \to 1$. For a multi-mode superposition the rate depends on the *total* energy difference $\Delta E = \sum_k (n_k - m_k)\hbar\omega_k$ as $\Gamma = G(\Delta E)^2 C_{\text{cube}}/(\hbar c^4 L)$: partially cancelling mode contributions reduce the decoherence, reinforcing ones enhance it.

J.3 Application to inflationary perturbations

Physical arguments suggest the same formalism gives a universal self-gravitational route to the quantum-to-classical transition of primordial perturbations. During slow-roll inflation a scalar mode squeezed after horizon crossing has mean occupation $\bar{n}_k \approx \frac{1}{4}e^{2N_k}$, with N_k the e-folds since crossing; its gravitational self-energy, evaluated with the Newtonian kernel over a Hubble volume, grows as $E_G(k) \sim (G\hbar^2 H_{\rm inf}^3/c^5)\, e^{4N_k}/16$. Setting $\Gamma_k = E_G(k)/\hbar$ equal to the Hubble rate gives

$$N_{\rm dec} = \frac{1}{4}\ln\Big(\frac{16}{\varepsilon_{\rm grav}}\Big), \qquad \varepsilon_{\rm grav} \equiv \Big(\frac{\hbar H_{\rm inf}}{E_P}\Big)^2, \tag{111}$$

e-folds after horizon crossing. For GUT-scale inflation ($H_{\rm inf} \sim 10^{13}$ GeV), $\varepsilon_{\rm grav} \approx 6.7 \times 10^{-13}$ and $N_{\rm dec} \approx 7.7$—well before recombination for all observable modes. This is a motivated order-of-magnitude estimate for the classicalization of primordial perturbations, with the same parametric dependence on $(H_{\rm inf}/M_P)^2$ as environmental decoherence but from the self-gravitational field alone, subject to $O(1)$ corrections from the de Sitter kernel and gauge choice: the de Sitter propagator differs from the Newtonian kernel only at super-Hubble separations (affecting the coefficient, not the scaling; for a local computation of superposition decoherence on a de Sitter background see [42]), and the gauge-dependence of T^{00} shifts only the $O(1)$ prefactor. The power spectrum, set by the diagonal density-matrix elements, is unaffected by decoherence, consistent with standard inflationary predictions.

K The Geometric Double Integral

The gravitational self-energy of a uniform density distribution in a cube of side L requires the double integral

$$\mathcal{J}(L) = \int_0^L\int_0^L\int_0^L\int_0^L\int_0^L\int_0^L \frac{dx\,dy\,dz\,dx'\,dy'\,dz'}{\sqrt{(x-x')^2+(y-y')^2+(z-z')^2}}\,. \tag{112}$$

Dimensional analysis fixes $\mathcal{J}(L) = C_{\rm cube}\,L^5$ for a dimensionless constant $C_{\rm cube}$.

Convergence. The integrand $1/r$ is integrable in $\mathbb{R}^3$: the volume element $d^3x\,d^3y$ scales as $r^5\,dr$ near the diagonal $\mathbf{x}=\mathbf{y}$, overcoming the $1/r$ singularity. The integral is finite without regularization.

Numerical value. Chandrasekhar [43] computed the constant for gravitational self-energy, verified by Ciftja [44], who evaluated the same $1/r$ double integral in closed form:

$$C_{\rm cube} = \frac{\mathcal{J}(L)}{L^5} \approx 1.19189\,. \tag{113}$$

A uniform sphere of radius R and mass M has self-energy integral $\int\!\int \rho^2/|\mathbf{x}-\mathbf{y}|\,d^3x\,d^3y = \frac{6}{5}\,M^2/R$ (gravitational self-energy $U = \frac{1}{2}G\int\!\int \rho^2/r = \frac{3}{5}GM^2/R$), i.e. $C_{\rm sphere} = 6/5 = 1.200$ in the normalization $\int\!\int \rho^2/r = C\,M^2/R$. This is close to the cube value $C_{\rm cube} \approx 1.192$ in the same normalization, reflecting the approximate shape-independence of the gravitational self-energy for compact objects.

References

[1] Jacob D. Bekenstein. Black holes and entropy. *Phys. Rev. D*, 7:2333–2346, 1973.

[2] Stephen W. Hawking. Particle creation by black holes. *Commun. Math. Phys.*, 43:199–220, 1975.

[3] Shinsei Ryu and Tadashi Takayanagi. Holographic derivation of entanglement entropy from AdS/CFT. *Phys. Rev. Lett.*, 96:181602, 2006.

[4] Juan Maldacena and Leonard Susskind. Cool horizons for entangled black holes. *Fortschr. Phys.*, 61:781–811, 2013.

[5] Lajos Diósi. A universal master equation for the gravitational violation of quantum mechanics. *Phys. Lett. A*, 120:377–381, 1987.

[6] Roger Penrose. On gravity's role in quantum state reduction. *Gen. Relativ. Gravit.*, 28:581–600, 1996.

[7] M. Sperzel. Holographic cosmology: Dark energy and the arrow of time from one horizon entropy budget, 2026. Companion paper, Quantum-Geometric Correspondence series.

[8] Stephen W. Hawking. Breakdown of predictability in gravitational collapse. *Phys. Rev. D*, 14:2460–2473, 1976.

[9] Geoffrey Penington. Entanglement wedge reconstruction and the information paradox. *JHEP*, 09:002, 2020.

[10] Netta Engelhardt and Aron C. Wall. Quantum extremal surfaces: holographic entanglement entropy beyond the classical regime. *JHEP*, 01:073, 2015.

[11] Ahmed Almheiri, Thomas Hartman, Juan Maldacena, Edgar Shaghoulian, and Amirhossein Tajdini. The entropy of Hawking radiation. *Rev. Mod. Phys.*, 93:035002, 2021.

[12] Venkatesa Chandrasekaran, Roberto Longo, Geoff Penington, and Edward Witten. An algebra of observables for de Sitter space. *JHEP*, 02:082, 2023.

[13] Edward Witten. Gravity and the crossed product. *JHEP*, 10:008, 2022.

[14] Ted Jacobson. Thermodynamics of spacetime: The Einstein equation of state. *Phys. Rev. Lett.*, 75:1260–1263, 1995.

[15] Joseph J. Bisognano and Eyvind H. Wichmann. On the duality condition for quantum fields. *J. Math. Phys.*, 17:303–321, 1976.

[16] Gerard 't Hooft. Dimensional reduction in quantum gravity. 1993.

[17] Leonard Susskind. The world as a hologram. *J. Math. Phys.*, 36:6377–6396, 1995.

[18] Raphael Bousso. The holographic principle. *Rev. Mod. Phys.*, 74:825–874, 2002.

[19] Fermi LAT and GBM Collaborations. A limit on the variation of the speed of light arising from quantum gravity effects. *Nature*, 462:331–334, 2009.

[20] Shuang-Nan Zhang et al. Detailed polarization measurements of the prompt emission of five gamma-ray bursts. *Nat. Astron.*, 3:258–264, 2019.

[21] Martin C. Weisskopf et al. The Imaging X-ray Polarimetry Explorer (IXPE): Pre-launch. *J. Astron. Telesc. Instrum. Syst.*, 8:026002, 2022.

[22] Richard P. Feynman and Frank L. Vernon Jr. The theory of a general quantum system interacting with a linear dissipative system. *Ann. Phys.*, 24:118–173, 1963.

[23] Amir O. Caldeira and Anthony J. Leggett. Path integral approach to quantum Brownian motion. *Physica A*, 121(3):587–616, 1983.

[24] Hiroki Takeda, Shogo Tomizuka, and Takahiro Tanaka. Gravitationally induced quantum decoherence of macroscopic objects. *arXiv preprint*, 2026.

[25] Charis Anastopoulos and Bei-Lok Hu. A master equation for gravitational decoherence: probing the textures of spacetime. *Class. Quantum Grav.*, 30:165007, 2013.

[26] Miles Blencowe. Effective field theory approach to gravitationally induced decoherence. *Phys. Rev. Lett.*, 111:021302, 2013.

[27] Bryce S. DeWitt. Quantum theory of gravity. i. the canonical theory. *Phys. Rev.*, 160:1113–1148, 1967.

[28] Roy J. Glauber. Coherent and incoherent states of the radiation field. *Phys. Rev.*, 131:2766–2788, 1963.

[29] Donald Marolf. Refined algebraic quantization: Systems with a single constraint. 1995.

[30] Domenico Giulini and Donald Marolf. On the generality of refined algebraic quantization. *Class. Quantum Grav.*, 16:2479–2488, 1999.

[31] Don N. Page and William K. Wootters. Evolution without evolution: Dynamics described by stationary observables. *Phys. Rev. D*, 27:2885–2892, 1983.

[32] Joseph J. Bisognano and Eyvind H. Wichmann. On the duality condition for a Hermitian scalar field. *J. Math. Phys.*, 16:985–1007, 1975.

[33] Thomas Faulkner, Robert G. Leigh, Onkar Parrikar, and Huajia Wang. Modular Hamiltonians for deformed half-spaces and the averaged null energy condition. *JHEP*, 09:038, 2016.

[34] Lajos Diósi. Models for universal reduction of macroscopic quantum fluctuations. *Phys. Rev. A*, 40:1165–1174, 1989.

[35] Frigyes Károlyházy. Gravitation and quantum mechanics of macroscopic objects. *Nuovo Cim. A*, 42:390–402, 1966.

[36] Yidong Chen, Nima Lashkari, and Kwing Lam Leung. Local approximations of global Hamiltonian from inclusion of algebras. *arXiv preprint*, 2026.

[37] Gaoping Long and Cong Zhang. Quantum geometry effects in quantum field theory: Hamiltonian constraint generates gravity–matter entanglement. 2026. arXiv:2602.14282.

[38] Charles W. Misner, Kip S. Thorne, and John Archibald Wheeler. *Gravitation*. W. H. Freeman, San Francisco, 1973.

[39] Norman Margolus and Lev B. Levitin. The maximum speed of dynamical evolution. *Physica D*, 120:188–195, 1998.

[40] L. Mandelstam and Ig. Tamm. The uncertainty relation between energy and time in non-relativistic quantum mechanics. *Journal of Physics (USSR)*, 9:249–254, 1945. Reprinted in: *Selected Papers*, Springer (2005).

[41] Seth Lloyd. Ultimate physical limits to computation. *Nature*, 406:1047–1054, 2000.

[42] Ran Li. Note on the local calculation of decoherence of quantum superpositions in de sitter spacetime. *Phys. Rev. D*, 111:044022, 2025. arXiv:2501.00213.

[43] Subrahmanyan Chandrasekhar. *Ellipsoidal Figures of Equilibrium*. Yale University Press, New Haven, 1969.

[44] Orion Ciftja. Coulomb self-energy of a uniformly charged three-dimensional cube. *Phys. Lett. A*, 375:766, 2011.